DEPARTAMENTO DE CIÊNCIAS DA

FACULDADE DE CIÊNCIAS E
TECNOLOGIA

Role of Sirtuin 3 on Doxorubicin-induced Toxicity on H9c2 Cardiomyoblasts

ANA RAQUEL LIGEIRO COELHO

2014

DEPARTAMENTO DE CIÊNCIAS DA VIDA

FACULDADE DE CIÊNCIAS E TECNOLOGIA
UNIVERSIDADE DE COIMBRA

Role of Sirtuin 3 on Doxorubicin-induced Toxicity on H9c2 Cardiomyoblasts

Dissertação apresentada à Universidade de Coimbra para cumprimento dos requisitos necessários à obtenção do grau de Mestre em Biologia Celular e Molecular, realizada sob a orientação científica do Doutor Paulo Jorge G. S. da Silva Oliveira (Centro de Neurociências e Biologia Celular) e com supervisão académica do Professor Doutor António Joaquim Matos Moreno (Universidade de Coimbra)

ANA RAQUEL LIGEIRO COELHO

2014

Work performed at the MitoXT - Mitochondrial Toxicology and Experimental Therapeutics Laboratory at the Center for Neuroscience and Cell Biology, University of Coimbra, under the guidance of Paulo J. Oliveira, PhD and Teresa L. Serafim, PhD.

The work was also performed under the academic supervision of António J. Moreno, PhD.

The present work was funded by the Portuguese Foundation for Science and Technology, research grant PTDC/SAU-TOX/110952/2009, Pest-C/SAU/LA0001/2013-2014, co-funded by FEDER/Compete/National-Funds.

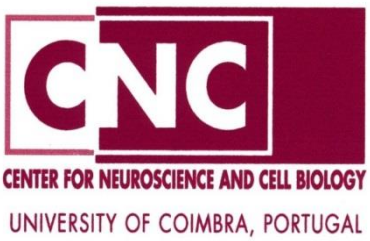

Statement of Originality

I hereby declare that the present work is the product of my own work. I declare that, to the best of my knowledge, my thesis does not infringe upon anyone's copyright nor violate any proprietary rights. I declare that this is a true copy of my thesis, including any final revisions, as approved by my supervisors, and that this thesis has not been submitted for a higher degree to any other University or Institution.

Acknowledgements

A realização desta Tese de Mestrado não teria sido possível sem a colaboração e o suporte de diversas pessoas. Após um intenso ano de aprendizagem e crescimento, gostaria de agradecer a todos aqueles que de alguma forma contribuíram para que esta etapa se tenha tornado realidade.

Em primeiro lugar, gostaria de agradecer ao meu orientador, Paulo Oliveira, por ter contribuído para o meu crescimento académico e pessoal ao longo deste ano. A oportunidade que me deu para trabalhar no seu grupo foi incrível. Obrigada por todo o empenho e dedicação.

À minha co-orientadora, Teresa Serafim, que foi imprescindível para me ajudar a ultrapassar todos os obstáculos com que me deparei ao longo deste percurso. Obrigada pela amizade e pelo conhecimento transmitido.

A todos os que de alguma forma estiveram relacionados com o meu trabalho, aos Professores, à Professora Emília Duarte e em especial a todos os elementos do meu Grupo de Investigação, com os quais criei uma amizade.

A todos os meus amigos da ESN Coimbra, em especial à Diana e à Marta, pelas experiências únicas vividas ao longo deste ano. Pelos momentos bons, mas também pelos menos bons, por os quais passámos e que nos fizeram crescer em conjunto.

Aos amigos que criei em Coimbra ao longo dos 6 anos. Pelos momentos felizes que aqui passámos, pelos sorrisos, gargalhadas, pelas Queimas e Latadas, por cada história que temos para recordar. Cada um, ao seu jeito, fez com que estes se tornassem os melhores anos. Aos meus grandes amigos: Bruno, Margarida, Pombo, Ana, Elvira, Sara, Heloísa, Bárbara, Zé Paulo, Jota, Maça… E a todos os restante amigos de licenciatura, mestrado ou apenas de Coimbra.

Aos meus amigos de Leiria, em especial aos BUS, por tornarem a minha vida num turbilhão de emoções e por estarem sempre lá, mesmo que nem sempre seja possível estarmos fisicamente presentes. Por todos os momentos que passámos desde a infância e por ainda sermos o que somos hoje. Ao Bernardo, à Rita e a todos os outros sem

qualquer excepção. Apenas salientar a minha inquilina ao longo deste ano, Jô, pelos grandes momentos que tivemos e pela companhia.

Às minhas amigas de sempre: Patrícia e Kristen. Por me aturarem e por estarem sempre incansavelmente comigo.

Um obrigada especial ao Rodrigo, por todos os momentos que partilhámos, por todos os sorrisos e pelo que crescemos juntos.

À minha família por todo o apoio incondicional. Aos meus avós por estarem sempre presentes e por terem tido um papel tão importante na educação de todos os netos. Aos meus tios e aos meus primos, que sempre foram como meus irmãos, em especial ao Guilherme e à Inês. Aos pequenos: Zé, Maria, Manel e Clarinha pelos momentos felizes que nos proporcionam. À minha Tia Cila por todo o apoio e por ter sido uma segunda mãe. Em especial aos meus pais pelo apoio incondicional e pelo carinho. Pela excelente educação que me deram e por todos os esforços que fizeram a pensar em mim. Sem vocês não teria sido possível atingir os meus objectivos e superar os obstáculos ao longo de todo o meu percurso, não só académico como também pessoal. Todos os objectivos que já alcancei e todos os sucessos que possa vir a ter, devem-se a vocês e são também para vocês.

As mais sinceras desculpas pelo facto de me arriscar a esquecer de algumas pessoas.

A todos vós, obrigada por fazerem parte.

Index

Abbreviations

AceCS2	Acetyl-CoA Synthase 2
Acetyl CoA	Acetyl Coenzyme A
ADP	Adenosine Diphosphate
AIF	Apoptosis-inducing Factor
ALDH2	Aldehyde Dehydrogenase 2
AMPK	AMP-activated Protein Kinase
ANT	Adenine Nucleotide Translocase
APS	Ammonium Persulfate
ATP	Adenosine Triphosphate
Bad	Bcl-2-associated Death Promoter
Bak	Bcl-2 Homologous Antagonist Killer
Bax	Bcl-2-associated X protein
Bcl-2	B-cell lymphoma 2
Bcl-XL	B-cell Lymphoma-extra-large
BSA	Bovine Serum Albumin
Cyp D	Cyclophilin D
Cyt c	Cytochrome C
DMEM	Dulbecco's Modified Eagle's Medium
DOX	Doxorubicin
Drp1	Dynamin-related Protein
ECF	Enhanced Chemi-Fluorescence
EDTA	Ethylenediaminetetraacetic Acid
eNOS	Endothial NO Synthase
ERK 1/2	Extracellular Signals Regulated Kinases 1/2
ETC	Electron Transport Chain
EV	Empty Vector
FBS	Fetal Bovine Serum

Fis1	Mitochondrial Fission 1 Protein
GDH	Glutamate Dehydrogenase
GTP	Guanosine Triphosphate
HMGCS2	Hydroxyl-3-Methylglutaryl-CoA Synthase
HSF-1	Heat-Shock Factor 1
hSirt3	Sirtuin 3 Wild-type Plasmid
hSirt3 mutant	Deacetylase Catalytically inactive Construct
Hsp25	Heat-Shock Protein 25
IDH2	Isocitrate Dehydrogenase 2
IMM	Inner Mitochondrial Membrane
LCAD	Long-Chain Acyl-Coenzyme A Dehydrogenase
LKB1	Liver Kinase B1
Mfn1	Mitofusin 1
Mfn2	Mitofusin 2
MPT	Mitochondrial Permeability Transition
mtDNA	Mitochondrial DNA
mTOR	Rapamycin
NAD	Nicotinamide Adenine Dinucleotide
nDNA	Nuclear DNA
NRT	cDNATemplate
NTC	Non-Template Control
OGC1	8-Oxoguanine-DNA Glycosylase 1
OMM	Outer Mitochondrial Membrane
OPA1	Optic Atrophy 1
OTC	Ornithine Transcarbamoylase
OXPHOS	Oxidative Phosphorylation
PBS	Phosphate Buffered Saline
PcDNA	Empty Vector
PGC-1α	Peroxisome Proliferator-activated Receptor-gamma Coactivator 1 alpha
PMSF	Protease Inhibitor Cocktail

PVDF	Polyvinylidene Difluoride membrane
RCR	Respiratory Control Ratio
ROS	Reactive Oxygen Species
SDS	Sodium Dodecyl Sulfate
Sir	Silent Information Regulator Proteins
siRNA	Small Interfering RNA
Sirt	Sirtuin
SOD	Superoxide Dismutase
SR	Sarcoplasmic Reticulum
SRB	Sulforhodamine B
sSirt3	Small Interfering RNA Sirt3
TBS-T	Tris-Buffered Saline Tween
TCA	Tricarboxylic Acid
TEMED	N,N,N',N'-Tetramethyllenediamine
TIM	Tranlocase of the Inner Membrane
TLRs	Toll-like Receptors
TOM	Tranlocase of the Outer Membrane
VEGF	Vascular Endothelial Growth Factor

Abstract

The anthracycline Doxorubicin (DOX) is one of the most widely used anti-neoplastic agents. However, treatment with this drug is associated with a cumulative and dose-dependent cardiotoxicity. Mitochondrial Sirtuin 3 (Sirt3) is the major mitochondrial deacetylase, modulating several pathways, such as apoptosis and metabolism. Thus, our hypothesis is that mitochondrial Sirt3 activity decreases DOX-induced cardiotoxicity. H9c2 cardiomyoblasts were transfected with siRNA and a plasmid construct to produce Sirt3 knock-down and Sirt3 overexpressing cells, respectively. DOX (0.5μM and 1μM) toxicity was evaluated by the Sulforhodamine B assay and by flow cytometry using the Life/Death assay. Mitochondrial depolarization and superoxide production was determined by fluorescence microscopy and content in specific proteins by western blot. Sirt3 overexpression or knock-down was confirmed by Western Blot and qRT-PCR. In all experimental groups, DOX induced cell death. Increase in Sirt3 content by transfection-mediated overexpression appeared to decrease DOX toxicity, most by maintaining the integrity of mitochondrial network and reducing oxidative stress. On the other hand, p53 seems to be a direct target of Sirt3 and the protection against cell death conferred by Sirt3 could be related to this protein.

Keywords: Sirtuin 3, Doxorubicin, Cardiotoxicity, Cell Death, Protection

Resumo

A antraciclina Doxorrubicina (DOX) é um dos mais usados agentes antineoplásicos. No entanto, o tratamento com este composto está associado com cardiotoxicidade, que é dependente da dose e da sua acumulação. A mitocondrial Sirtuína 3 (Sirt3) é a maior deacetilase mitocondrial, modulando diversas vias, tal como a apoptose e o metabolismo celular. Assim a nossa hipótese é que a actividade da Sirt3 diminui a cardiotoxicidade induzida pela DOX. Os cardiomioblastos H9c2 foram transfectados com siRNA e plasmídeos para produzir células com Sirt3 silenciada e sobreexpressa, respectivamente. A toxicidade da DOX (0.5 e 1 μM) foi avaliada pelo ensaio da Sulforodamina B e por citometria de fluxo. A despolarização mitocondrial e a produção do anião superóxido foi determinada por microscopia de fluorescência e o conteúdo de proteínas específicas por western blot. A sobre e sub-expressão da Sirt3 foi confirmada por western blot e RT-PCR. A toxicidade da DOX envolveu a indução de morte celular em todos os grupos. O aumento do conteúdo de Sirt3 mediado pela sobreexpressão parece diminuir a toxicidade da DOX, maioritariamente pela manutenção da integridade da rede mitocondrial e redução do stress oxidativo. Por outro lado, a p53 parece ser um alvo directo da Sirt3 e a protecção conferida contra a morte celular pela Sirt3 pode ser relacionada com esta proteína.

Palavras-chave: Sirtuína 3, Doxorrubicina, Cardiotoxicidade, Morte Celular e Protecção

Chapter 1 - Introduction

1. Mitochondria

1.1 Mitochondrial Structure and Organization

Mitochondria were first described in 1857 by Rudolf Koelliker, with Carl Brenda giving them the name "mitochondria" a few years later [1]. Mitochondria are composed by two membranes, the outer mitochondrial membrane (OMM) and the inner mitochondrial membrane (IMM), which contains invaginations, called cristae. The cristae allow for a greater surface area, which is correlated with metabolic activity. The arrangement of these membranes forms the intermembrane space, located between both membranes, and the matrix that is enclosed by the IMM [2]. Multisubunit translocases are located in both mitochondrial membranes and play a role in recognition and transport of several proteins. The translocase of the outer membrane (TOM) recognizes mitochondrial-target proteins and forms a pore which allow the cross of outer membrane. Proteins targeted to the matrix interact with translocases of the inner membrane (TIM) [3].

Advances in imaging techniques showed mitochondria as a dynamic organelle that undergo fission and fusion, allowing its movement through microtubule network and size and shape changes [2, 4]. Beyond influencing mitochondrial morphology, mitochondrial fission-fusion can contribute to repair defective mitochondria, segregation of mitochondria into daughter cells, efficiency of oxidative phosphorylation (OXPHOS) and mitochondrial calcium signaling. This process is mediated by several proteins that promote the remodeling of OMM and IMM, such as dynamin-related protein (Drp1) and mitochondrial fission 1 protein (Fis1) for fission and mitofusin 1 (Mfn 1)/2 (Mfn2) and optic atrophy 1 (OPA1) for fusion [5].

Mitochondria also has its own genome, exclusively maternally inherited. Mammalian mitochondrial DNA (mtDNA) is 16.6 kb circular double-stranded molecule capable of transcription, translation and protein synthesis, independently of nuclear DNA (nDNA). It encodes 22 rRNAs, 2 rRNAs and 13 subunits from OXPHOS complexes I, III, IV and V [4, 6].

1.2 Mitochondrial Bioenergetics

Mitochondria are the *cell's powerhouse*, once they produce the majority of cellular adenosine triphosphate (ATP) and carry out several other crucial metabolic processes, such as tricarboxylic acid cycle, β-oxidation of fatty acids, urea cycle and pyruvate oxidation [7]. During glycolysis, glucose is converted to pyruvate in cytosol, reducing cytosolic nicotinamide adenine dinucleotide (NAD^+) to NADH, being then transported to mitochondria. In the mitochondrial matrix, pyruvate undergoes an oxidative decarboxylation to acetyl coenzyme A (acetyl CoA) by pyruvate dehydrogenase complex. Fatty acids are also oxidized in mitochondria via β-oxidation to generate acetyl CoA, NADH + H^+ and succinate. Acetyl CoA enters in the Krebs cycle or Tricarboxylic Acid (TCA) cycle, producing for each round 2 molecules of CO_2, 3 molecules of NADH, 1 molecule of succinate and 1 molecule of guanosine triphosphate (GTP) [2].

The next stage is OXPHOS, in which respiratory substrates, such as NADH and succinate generated through the TCA cycle, are oxidized and coupled to the production of ATP. In this process, substrate oxidation is performed to respiratory enzyme complexes that are capable of accepting and donating electrons and are located in the IMM. Initially, 2 electrons are transferred from NADH to NADH dehydrogenase (complex I) or from succinate to succinate dehydrogenase (complex II) with $FADH_2$ as a co-factor, reducing ubiquinone to ubiquinol. After, electrons are transported to cytochrome c reductase (complex III) and then cytochrome c transfers electrons to cytochrome c oxidase (complex IV), reducing molecular oxygen, the final acceptor, to form H_2O. The energy released by the transfer of electrons is coupled to the translocation of protons from the matrix to intermembrane space, by complex I, III and IV [7]. The resulting proton gradient, called proton-motive force, composed by an electric and a pH-dependent component, is used to drive the synthesis of ATP via ATP synthase (complex V). During this process, ATP is produced, with part being used by mitochondria and the majority being transported to the cytosol in exchange for cytosolic adenosine diphosphate (ADP) by the enzyme adenine nucleotide translocase (ANT) [8].

1.3 Mitochondria: More than Cell's Powerhouse

The contribution of mitochondria to cellular physiology is not limited to ATP production. Mitochondria are also crucial for the regulation of intracellular calcium homeostasis and for the production of reactive oxygen species (ROS) and reactive nitrogen species, which are involved in cell signaling but can also be harmful at certain concentrations to the cell [9, 10].

Cytosolic calcium alterations provide signals to control several cellular events, such as muscle contraction, neurotransmitter release and cell death [11]. On the other hand, mitochondrial calcium is essential for mitochondrial function and ATP synthesis. Mitochondrial calcium accumulation is performed by a specific non-ATP dependent uniporter. Calcium efflux results from an exchanged with Na^+ or H^+, depending on the tissue. The accumulation of calcium in the matrix depends on the proton gradient, generated by respiratory chain. This accumulation stimulates mitochondrial NADH generation and ATP synthase, increasing ATP production [8, 12].

The mitochondrial electron transport chain (ETC) is a main source of ROS production, namely from complex I and III [13]. Complex II can influence the ROS production by complexes I and III, but more recently it was proposed that complex II controls ROS production by itself [14]. The generation of ROS during normal physiology seems to be a natural consequence of metabolism and is necessary for cellular pathways, for example for vascular endothelial growth factor (VEGF) signaling [15]. During OXPHOS, a small percentage of oxygen is converted in superoxide radical anion, which is converted into hydrogen peroxide, a relatively inert molecule, by superoxide dismutase (SOD). Three forms of SOD are present in humans [16]. Although all SODs catalyze the same reaction, they not share a primary structure. The cytosolic SOD I contains a Cu-Zn prosthetic group and SOD III is tretameric and is extracellular [17]. Mitochondria are also equipped with enzymatic defenses, such as manganese-SOD (SOD II) and glutathione, although stress conditions can deregulate this process and increase ROS production. Increased oxidative stress results in mitochondrial proteins damage, lipid peroxidation and mtDNA alterations, which promotes loss of mitochondrial integrity [8].

Beyond mitochondrial calcium overload and oxidative stress, another deleterious condition for mitochondria is the mitochondrial permeability transition (MPT). This phenomenon is characterize by an increased permeability of the IMM, which allows the free passage of smaller molecules, resulting in a bigger osmotic pressure that leads to mitochondrial swelling. If the MPT opening is persistent, mitochondrial membrane depolarization and OXPHOS uncoupling can occur, leading to cell death [18].

1.4 Mitochondria and Cell Death

Multiple forms of cell death can be triggered during mitochondrial stress, such as apoptosis, necrosis and mitophagy. The removal of damaged mitochondria can lead to cell survival in an adaptive process or to cell death. This process, called mitophagy, seems to be stimulated by MPT and OMM permeabilization [9]. Both necrosis and apoptosis can be initiated by internal as well as by external stimuli and might involve activation of similar signaling pathways such death receptors or OMM permeabilization. However, the mode of cell death is determined by the intensity of the insult and the availability of ATP [9, 16]. Necrosis can occur due the activation of the MPT pore, which compromises ATP production, once the IMM becomes freely permeable to protons, leading to OXPHOS uncoupling. A trait of necrosis is a drastic drop of ATP and inflammation. Apoptosis involves the activation of specific proteases called caspases, which are divided in initiator caspases (2, 8, 9 and 10) and effector caspases (3, 6 and 7). Mitochondria are crucial in the intrinsic pathway, which is characterized by intracellular apoptotic stimuli. With the rupture of the OMM, several apoptotic initiators, such as cytochrome c (Cyt c), apoptosis-inducing factor (AIF) and SMAC/DIABLO, are released from the intermembrane space. Pro-apoptotic proteins, including Bcl-2-associated X protein (Bax) and Bcl-2 homologous antagonist killer (Bak), can also form channels, allowing the release of those initiators. During normal situations the anti-apoptotic members of B-cell lymphoma 2 (Bcl-2) family avoid the release of pro-apoptotic members. However under stress an imbalance and inactivation of anti-apoptotic proteins occur. When cytochrome c is released, promoting cyt c – Apaf-1 – Pro-caspase 9 complex (called apoptosome) assembly, which in turn activates

caspases 9 and the caspases cascade is triggered. Activated caspase 3, 6 and 7 cleave a number of targets, such as lamins and PARP, leading to apoptosis [12, 19, 20].

1.5 Mitochondrial Drug-Induced Toxicity

Some clinically used drugs cause side effects, usually observed in patients with mitochondrial diseases [21]. It has become clear that several chemical agents can disturb mitochondrial function. Nowadays, 30% of new drugs fail to reach the market as a result of toxicity issues, namely associated to mitochondria [22]. Drug-induced mitochondrial dysfunction can be caused by the parent drug itself or to reactive metabolites produced by cytochrome P450. The critical role of mitochondria in cellular bioenergetics and its complexity makes mitochondria a crucial player in the development of drug-induced toxicity [23]. Mitochondrial injury can include alterations of metabolic pathways and damage on mitochondrial components, such as OXPHOS uncoupling ETC, inhibition of OXPHOS complexes, oxidative stress, opening of MPT pore, depletion of mtDNA, inhibition of TCA cycle and β-oxidation and inhibition of membrane transporters [21-23]. Mitochondrial dysfunction has been associated with the toxicity of several anti-cancer drugs, including Doxorubicin that will be discussed in the following section.

2. Doxorubicin

2.1 Anthracyclines

Anthracycline drugs were first identified in the 1950's from the soil bacterium *Streptomyces peucetius* [24]. This antibiotic family is composed by four main anthracyclines: Doxorubicin (Fig. 1), Daunorubicin, Epirubicin and Idarubicin [25]. These molecules are highly effective anti-neoplastic agents and are used to treat numerous adult and pediatric cancers. Recognized as a potent antitumor agent, DOX has been used (alone or in combination with other agents) in treatments against a wide range of solid tumors and hematologic malignancies, such as breast cancer, leukemia and lymphoma [24, 26].

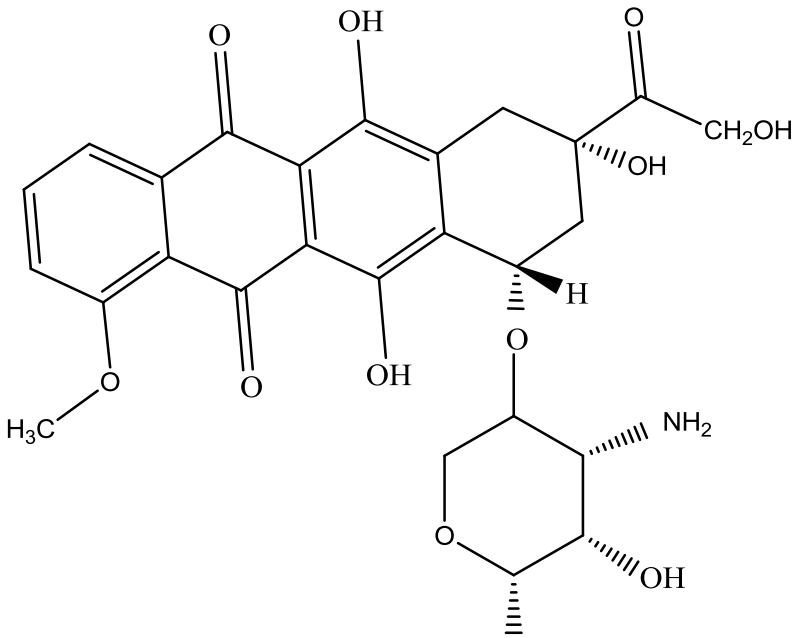

Figure 1 - Chemical Structure of Doxorubicin. Figure drawn through ChemBioDraw software.

2.2 Antineoplastic Mechanisms

Despite the extensive use of DOX, the antineoplastic mechanism still raises controversy, due to the combination of several mechanisms. Initially, the mechanism for anti-cancer effects was attributed to intercalation of the planar DOX ring into DNA helix, which unwind nuclei acids and cause stereochemical disorder, blocking transcription and replication and preventing the rapidly growing of cancer cells. DOX covalently binds to proteins involved in DNA replication and transcription, leading to an inhibition of DNA, RNA and protein synthesis, inducing cell death [26, 27]. Topoisomerase II is in fact recognized as a main cellular target. DOX also acts by stabilizing a reaction in which DNA strands are cut and covalently linked to the enzyme, blocking consequent DNA resealing. This mechanism blocks further DNA replication and transcription [26]. Similarly to other anti-neoplastics, DOX administration causes adverse reactions through multiple mechanisms and targets [25].

2.3 Treatment-Related Toxicity

Albeit controversial, it is now accepted that DOX-induced toxicity is independent from its anticancer activity [12]. The successful treatment with DOX is hampered by side-effects, such as hematopoietic suppression, nausea, vomiting, extravasation and

alopecia. However, the most feared complication is cardiotoxicity. Although several organs are affected, the heart seems to be the most affected one, with several possible explanation available, including: 1) a specific accumulation or differences in drug efflux; 2) a decreased on antioxidant levels in cardiac tissue or 3) a higher mitochondrial content and energetic demand of heart [12]. Because DOX is a very potent anti-neoplastic agent, the study of the mechanisms responsible for DOX-induced cardiotoxicity is needed, in order to potentially increase the effective dosage given to patients [27, 28].

2.3.1 Cardiotoxicity

The dose-dependent cardiotoxicity induced by DOX compromises the clinical application in its fullest effective dosage. The heart has a high energy demand and any interference in energy production machinery will affect the physiology and heart contraction. Indeed, DOX-induced cardiotoxicity has a strong mitochondrial component [12, 29]. As a result of DOX treatments, patients can develop acute, early- or late-onset cardiotoxicity. The acute toxicity (pericarditis and arrhythmias) appears immediately after treatment and usually reverts after ending the treatment; this probably resulting from an inflammatory response [27]. Early-onset cardiotoxicity arises about one year after chemotherapy with DOX and is characterized by the appearance of chronic dilated cardiomyopathy. Delayed DOX cardiotoxicity can develop after 10 or 15 years with a normal cardiac function and is characterized by left ventricular dysfunction and congestive heart failure [27, 30]. This is particularly important for adult survivors of pediatric malignancies. In a juvenile mouse model, it was demonstrated that when hearts were exposed to DOX, the development of an abnormal vasculature is observed, with hearts being more susceptible to myocardial infarction. Also, a decreased number of progenitor cardiac cells were observed after DOX treatment, suggesting that these undifferentiated cells are more susceptible to DOX, thus limiting the resistance of the heart to stress [31]. With a similar work, Angelis et al. reported different susceptibilities of adult and neonatal rat cardiomyocytes to DOX treatment, with the apoptotic pathway being more active in

immature cells, demonstrating again that cardiac cells respond differently to DOX depending on their differentiation state [32]; this was further confirmed by our group [27]. Besides age, gender is another risk factor in the side-effects of DOX. It was reported that females suffer a more severe cardiotoxicity with more depressed contractility. Simultaneous administration of other cardiotoxicity drugs and comorbidity, such as hypertension, diabetes mellitus, liver disease and previous cardiac disease, also contribute to an increased risk of cardiotoxicity [33]. The risk level can be identified as type I or Type II based on the effect on cardiomyocytes. The type I is characterized by cell death, necrosis or apoptosis and is not reversible, representing the late-onset cardiotoxicity. Type II involves reversible cardiomyocyte dysfunction [24]. The difference in time-of-onset suggests that different mechanisms are involved [28]. Different studies suggest a range of mechanisms that lead to chronic toxicity include: disruption of cellular and mitochondrial homeostasis, impaired expression of cardiac proteins, induction of mitochondrial DNA lesions, extracellular matrix remodeling, apoptosis induction and others [24-26]. However, DOX-induced oxidative stress on cardiac cells has been implicated as a major mechanism responsible for cardiotoxicity [34].

2.3.1.1 Mitochondria as the Origin of Cardiotoxicity: Oxidative Stress

The generation of reactive oxygen species is one of the most described mechanisms proposed for DOX cardiotoxicity. The ability to induce ROS was predicted from DOX chemical structure, which contains a quinone moiety [35, 36]. In mitochondria, DOX interacts with the electron transport chain (NADH dehydrogenase - complex I) as well as with other cellular dehydrogenases, such as cytochrome P450, being reduced to an unstable semiquinone, that can react with oxygen and generate ROS [12, 24]. Oxidative stress primarily affects mitochondria, once it is proposed that DOX presents a strong affinity to cardiolipin, one of the most abundant phospholipid in the IMM. Since cardiolipin is required for the activity of ETC enzymes, DOX-induced damage to cardiolipin results in the inhibition of oxidative phosphorylation [37]. mtDNA is damaged by ROS or directly by DOX leading to ECT failure and increase in ROS

release. Therefore, DOX-induced oxidative stress results in damage of mitochondrial structures, through protein and lipid peroxidation, oxidation of mtDNA and induction of the MPT pore [34]. Due to the impairment of ETC, Carvalho et al. reported a stimulation of glycolysis caused by DOX on cardiac cells, using a rat model of chronic DOX-induced cardiomyopathy [38]. Metabolic remodeling caused by DOX may occur when metabolic gene expression is transcriptionally suppressed or stimulated due to DOX treatment [28, 38]. The formation of DOX-iron complexes also favors hydroxyl radical generation through the Fenton reaction, acting through recycling ferric anion. However, in most cells, including cardiac, it is thought that not enough free iron exists to complex with DOX to an extent necessary to cause cardiomyopathy. Therefore, DOX may alter iron homeostasis, via aconitase [28]. The effects of DOX on iron metabolism can also be mediated by proteins that sequester and bind intracellular iron [12, 24, 28, 37]. In addition, DOX administration increase endothelial NO synthase (eNOS) and inducible NO synthase, resulting in unbalanced production of NO and consequent harmful effects. DOX can also be metabolized by NOS as well, leading to superoxide anion production [12]. In a sub-chronic DOX toxicity model, Pereira et al. demonstrated that cardiac mitochondria are more affected than their liver or kidney counterparts, with more alterations in terms of mitochondrial oxygen consumption and mitochondrial transmembrane potential [39]. In this work it is clear that in order to prevent cardiotoxicity, ROS production should be limited, without suppressing the anti-neoplastic activity.

Overexpression of mitochondrial SOD II decreases apoptosis and improves left ventricular function scavenging free radical in mitochondria [24]. Indeed, overexpression of SOD II in NO null mice prevents DOX side effects [40]. Besides inhibiting OXPHOS, ROS can induce the oxidation of some residues or functional groups, such as thiol groups which form disulfide bonds upon oxidation. This leads to conformational changes and consequently inhibition of function. Several mitochondrial proteins, including the adenine nucleotide translocase (ANT) undergo oxidation, which appear to be critical for the regulation of the calcium-dependent MPT pore [12, 41].

2.3.1.2 Mitochondria as the Origin of Cardiotoxicity: Intracellular Calcium Dysregulation

An interplay between calcium and ROS generation has already been demonstrated [28]. Some studies highlighted loss of mitochondrial calcium loading capacity through increased MPT pore induction as one aspect of DOX toxicity [28, 37]. Besides mitochondria, DOX can alter calcium homeostasis in muscle cells by disruption of normal sarcoplasmic reticulum (SR) function, inhibiting the Ca^{2+} ATPase pump and impairing calcium clearance systems. DOX can trigger the release of Ca^{2+} from the SR by increasing the probability of opening of ryanodine channels [28]. Saeki et al. proposed that DOX binds to several sites on the ryanodine channel and that this binding occurs regardless the channel being open or closed [42]. Under distress, the ER can trigger the activation of caspase 12, followed by apoptotic induction. Because a major component of intracellular calcium in cardiomyocytes is contained within the SR, oxidative stress leads to calcium leakage, calpain activation and caspase 12 cleavage [28, 43]. In this context, it is not surprising that DOX cardiomyopathy is associated with myofibrillar deterioration, which is also likely to be a consequence of calpain activation and titin degradation, one of the largest proteins and component of cardiac sarcomeres [28]. Lim et al. observed that calpain inhibition maintains sarcomeres and cardiac function after DOX treatment [44]. Mitochondria in cardiomyocytes are located near calcium-release sites on the SR and can capture a large quantity of calcium [45]. DOX increases the susceptibility of mitochondria to calcium, decreasing the ability to retain it, contributing to disturb cytosolic calcium levels. As described above, excessive mitochondrial calcium accumulation triggers MPT pore, increasing the permeability of the IMM and disrupting energy-generating processes [12, 30, 37].

2.3.1.3 Mitochondria as the Origin of Cardiotoxicity: Bioenergetics Alterations

There are evidences that correlate DOX cardiotoxicity with disturbances of heart mitochondrial function and bioenergetics. Oxidation of mtDNA results in a defective respiratory chain that will enhance electron leak to molecular oxygen, increasing ROS production, which can directly inhibit the complexes of OXPHOS [12]. On the other hand, DOX forms complexes with cardiolipin, disturbing complex activity. Then DOX interacts directly with complex I undergoing a quinone moiety reduction, inducing ROS formation [46]. Some authors described that alterations of mitochondrial bioenergetics were detected right after the oxidative imbalance was established [47, 48]. Using different models, it has been observed that DOX administration compromises respiratory function of cardiac mitochondria, with a decrease in state 3 respiration rate and stimulation of respiratory state 4 [39, 49, 50]. Interestingly, state 3 alterations in DOX-treated rats were reversed by dithiothreitol, which suggest specific alterations in protein thiol groups by DOX [51]. Consequently, the respiratory control ratio (RCR) was significantly lower, suggesting once more that DOX interferes with the fundamental regulation of OXPHOS. Some authors observed no impairment on ATP synthesis efficiency, as seen as a normal ADP/O ratio [50]. However recent studies showed that ATP synthase was significantly reduced in both H9c2 cells and mitochondrial homogenates, with an inhibition of FoF1 proton pump [46, 52]. The inhibition of others OXPHOS complexes, namely NADH dehydrogenase [46, 48, 50], succinate dehydrogenase [46, 48] and cytochrome c oxidase were also described [53, 54]. The inactivation of other mitochondrial enzymes also affected the mitochondrial bioenergetics state. A decrease on functional ANT, β-oxidation related enzymes and Reiske iron-sulfur protein, a ubiquitously expressed ETC component, resulted in a reduction of bioenergetics capacity [12]. Other enzymes that catalyzed reactions in TCA cycle are also affected, including enzymes present in α-ketoglutarate dehydrogenase and pyruvate dehydrogenase complexes [12, 46]. In fact, a significant increase in extracellular acidification and lactate production, a sob-product of

glycolysis, and the decrease in OXPHOS suggests a shift to glycolysis after DOX treatment [37, 46].

2.3.1.4 Mitochondria as the Origin of Cardiotoxicity: Apoptotic Signaling

It is accepted that many mechanisms such as MPT pore, ROS generation or mitochondrial dysfunction are involved in cardiotoxicity induced by DOX. Cardiomyocytes can undergo apoptosis, necrosis, autophagy or senescence. Autophagy might be triggered by energy depletion, ROS, mitochondrial depolarization, oxidized proteins and MPT induction, all traits present after DOX treatment. It is not known if autophagy is directly induced by DOX or is a consequence of mitochondrial dysfunction [12]. Cardiomyocyte apoptosis has been proposed as a mechanism by which DOX causes deterioration of cardiac function. Apoptosis is an energy-dependent programmed cell death, crucial for normal development and cell homeostasis. The cellular morphological changes include cell shrinkage, DNA fragmentation, chromatin condensation and membrane blebbing [30, 37]. DOX causes apoptosis through multiple mechanisms that apparently have mitochondria as initiators [28]. Interestingly, the expression of anti-apoptotic proteins (B-cell lymphoma-extra-large (Bcl-XL) and Bcl-2) is initially up-regulated after DOX treatment, suffering a secondary decrease [24]. ROS generation, which disrupts cardiolipin and leads to the MPT pore, can lead to the release from mitochondria of several apoptotic initiators, such as cytochrome c or the AIF. Pro-apoptotic factors such as Bax and Bak can be directed to mitochondria after treatment [12, 24]. The transcriptional factor GATA-4, important in myocardium development and function, regulates the apoptotic pathway by activating the anti-apoptotic gene Bcl-XL. In early stage of DOX treatment, GATA-4 depletion is observed, which subsequently enforces cardiomyocyte apoptosis [30, 55]. DOX also inhibits Akt phosphorylation increasing active GSK3β, a negative regulator of GATA-4 in the nucleus [56]. Dephosphorylation of Akt and Bcl-2-associated death promoter (Bad) can activate caspase 3, inducing DNA damage [37]. Kawamura et al. observed a depletion of cardiac p300 mRNA, a

transcriptional co-activator needed for the maintenance of the differentiated phenotype in hearts from DOX-treated mice. It was also reported that the overexpression of p300 prevented apoptosis and cardiac dysfunction induced by DOX [57]. Although normally cardiomyocytes are resistant to Fas-induced apoptosis, in the presence of DOX cardiomyocyte apoptosis can occur via Fas pathway [58]. Moreover, ROS activates the transcription factor NF-κB, exercising a pro-apoptotic effect via direct activation of apoptotic genes, such as FasL, Fas, c-Myc and p53 [59]. ROS also down-regulates the expression of FLIP, a caspase 8 inhibitory protein, which in part sensitizes Fas-mediated apoptosis [30]. According to Verdam, oxidative stress also activates heat-shock factor 1 (HSF-1), which acts to produce more heat-shock protein 25 (Hsp25) that stabilizes p53, increasing the production of pro-apoptotic proteins [60]. The heat-shock family of proteins has a different role in these processes. For example, Hsp27 prevents DOX-induced apoptosis and myocardial dysfunction and Hsp10 and Hsp60 increase pot-translational modifications of Bcl-2 proteins [61]. Some Heat shock proteins can also be secreted into the extracellular space and bloodstream, acting as ligands for toll-like receptors (TLRs). TLR-2 functions as a "death receptor" that activates the apoptotic apparatus, such as FADD and caspase-8, without a conventional cytoplasmic death domain. This TLR signaling through NF-κB pathway is involved in cytokine production, apoptosis and cardiac dysfunction after DOX treatment in vivo [28]. DOX can likewise directly influence caspases activity, activating caspase-3 [28] and caspase-9 [26]. Numerous studies have shown that DOX-induced cardiomyocyte apoptosis is also associated with increased expression and activation of p53 tumor suppressor protein, leading to transcriptional activation of pro-apoptotic protein [34].

2.3.2 DOX and p53

The transcription factor p53 is a short-lived protein with a half-life of 20-40 min being present at a low level under normal conditions. In the presence of DNA damage, p53 is activated and as a nuclear transcription factor, regulates several genes involved in cell cycle arrest, DNA repair and apoptosis [34, 37, 62]. p53-mediated signals in cardiomyocytes apoptosis are triggered by hypoxia, ischemia, heart failure or

mechanical stretch, being also activated by DOX [63]. Accumulation of DOX in the nucleus of cardiac cells and subsequent DNA damage was observed in DOX-induced cardiac myocyte death. In fact, DOX treatment seems to cause an increase in the active form of the DNA damage-activated p53 protein [34]. When exposed to DNA damage stress, p53 is phosphorylated in both the amino- and carboxyl- terminal domains, including at Ser15, leading to the stabilization and accumulation of p53 in the cytoplasm. Subsequently, it is trans-activated into the nucleus to induce the expression of some genes [62]. In addition, the acetylation of p53 at lysines 320 and 383 requires the previous phosphorylation of p53 at serine 15 and at additional amino-terminal sites, which further stimulates these acetylation events [64]. In the nucleus, p53 induces apoptosis through transcription-induced regulation of the expression of Bcl-2 family members, oxidative stress induction, mitochondrial cytochrome c release and caspase-3 activation [65]. DOX interference with DNA replication and transcription leads to p53 activation and translocation to mitochondrial membranes. In fact, increased levels of p53 in mitochondria and nuclei were measured in response to DOX, and its localization in mitochondria leads to mtDNA damage [34, 66]. DOX-activated p53 can also act as a transcription factor increasing the expression of pro-apoptotic cells, such as Bax, which is translocated to mitochondrial membranes and interferes with mitochondrial function, including by inducing mitochondrial membrane potential depolarization [34]. The increase of p53 expression is also associated with the downregulation of Bcl-2 [62], with Liu et al. associating an increase of PUMA in p53-mediated apoptosis *in vitro* and *in vivo*. p53 can bind to Bcl-XL protein, causing a conformational alteration and mitochondrial translocation of p53 and Bcl-2 that leads to the release of cyt c and cell apoptosis [34, 62]. DOX activation of mitochondrial p53 can also lead to HIF-1 inhibition and promote the decrease of cardiac mass [37]. ROS/RNS are critical inducers of p53 accumulation in the heart [67]. Shizukuda et al. (2005) observed that p53 KO mice are resistant to acute cardiotoxicity and myocardial glutathione and SOD I levels are preserved after DOX injection. Although this did not happen in WT mice, it suggests that p53 is important for DOX-induced cardiotoxicity and oxidative stress generation [63]. According to Liu et al. (2008), cytotoxic effects in H9c2 cells were also associated with the increased activation and nuclear translocation

of extracellular signals regulated kinases 1/2 (ERK1/2) and p53. ERK 1/2 is an important early mediator for DOX-induced cell apoptosis, operating upstream to p53 and phosphorylating p53 (Ser15) [62]. Acute DOX-induced cardiotoxicity can also result from p53-dependent deregulation of the mammalian target of rapamycin (mTOR), a serine/threonine protein kinase that controls protein translation and cell growth. Zhu et al. (2009) suggested that acute DOX-induced cardiac systolic dysfunction and loss of cardiomyocytes occurs via p53-dependent inhibition of mTOR. However cardiomyocyte apoptosis occurs via a p53 dependent pathway, but independent of mTOR signaling [68]. Using a chemical inhibitor of p53, pifithrin-α, Sardão et al. (2009) and Liu et al. (2004) observed a blockage of apoptosis via the inhibition of p53 downstream activity, affecting Bax and MDM2 expression, which are increased with DOX treatment [34, 69]. Cell death cause by DOX treatment was not completely inhibited, suggesting that p53-independent mechanisms are operating [70]. In p53-null osteosarcoma Saos-2 cells, DOX treatment induced apoptosis, leading to mitochondrial membrane depolarization, cytochrome c release, caspase-3 activation, up regulation of Bax and down regulation of Bcl-2. Oxidative stress was also increased and may be a signal for DOX-induced cell death even in the absence of p53, since the reduction of ROS lead to the suppression of the effects induced by DOX [65].

2.4 Prevention of Doxorubicin-Induced Cardiotoxicity

Oxidative stress has been proposed as the major mechanism of DOX-induced cardiotoxicity. Thus, free radical scavengers and other compounds with antioxidant properties have been used to mitigate DOX cardiotoxicity [71], these compounds include Vitamin E and N-acetyl cysteine [72]. Dithiol compounds, such as lipoic acid, prevent lipid and protein oxidation and prevent mitochondrial calcium dysregulation caused by DOX treatment [73]. Flavonoids are also potential protectors due to radical-scavenging and iron-chelating properties [74, 75]. Other hypothesis is the use of a calcium channel antagonist. Although several compounds were tested to decrease DOX-induced cardiotoxicity, the efficacy of those compounds is still far from complete. Thus, the use of DOX remains limited and more efforts are needed to find more

protective compounds. In this context, and since DOX-cardiotoxicity induces alterations in a large number of pathways, the modulation of protective mechanisms such as sirtuins can be a good approach to reduce this toxicity, due to their capacity of cellular metabolism regulation, oxidative stress and other pathways, as explained in the next section.

3. Sirtuins

3.1 Classification of Sirtuins

Sirtuins, or Silent information regulator proteins (Sir) were originally characterized in 1984 in yeast as regulators of life span. These proteins are present in a wide range of organisms, from bacteria to humans, forming a conserved family. In mammalians seven sirtuins homologues (Sirt1-7) have been identified, affecting several biological processes including longevity, aging, metabolism and the response to stress [76-78]. All seven sirtuins contain a conserved 275 amino acid catalytic core domain together with N-terminal and/or C-terminal domains. Based on the phylogenetic analysis of the core domain, the seven human sirtuin genes are included in four classes together with other Sir2-related proteins widely distributed in eukaryotes and prokaryotes: Sirt 1-3 are class I, Sirt 4 and Sirt 5 are class II and III, respectively, and Sirt 6 -7 belong to class IV. Additionally, a novel class "U" has been created to include sirtuins with unique features, such as gram-positive bacteria and Termoga maritime sirtuins [79].

3.2 Sirtuin Enzymatic Activity

The major enzymatic activity of all sirtuins, except Sirt 4, is protein deacetylation, in which the acetyl group of lysine is transferred from the target protein to the ADP-ribose component of NAD^+. Therefore, this reaction is dependent of NAD^+, consuming mole equivalent of NAD^+ per acetyl group removed and suggesting that sirtuins can be sensors of the cellular redox state and energy status [80]. The end result will be the deacetylation of proteins, 2'-O-acetyl-ADP ribose and nicotinamide. Sirt 4 and additionally Sirt 6 present ADP-ribosyl transferase activity, which are also dependent of NAD^+ [81]. Moreover, Sirt5 was recently shown to demalonylate and desuccinylate

proteins, specially the urea cycle enzyme carbamoyl phosphate synthetase 1 enzyme [82]. Sirtuins are regulated at different levels and their activity is altered facing their subcellular localization, transcriptional regulation, post-translational modifications and the substrate availability. In fact, the availability of NAD^+ is possibly the most important mechanism that regulates sirtuins activity. Variations in NAD^+ levels occur as the result of its synthesis and consumption [82]. For example, during metabolic stress (caloric restriction) NAD^+ increases leading to sirtuin activation [83]. Moreover, nutrients and other molecules affect directly or indirectly sirtuin activity. Nicotinamide, the reaction product, noncompetitively inhibits sirtuins, acting as an endogenous regulator [81]. Some chemical compounds also can act as sirtuins activators or inhibitors. Polyphenols are compounds produced by plants, with a well-known antioxidant activity, and are also sirtuins activators. Among the polyphenols, one important example is resveratrol [84]. Likewise oroxylin A, a Chinese medicinal plant, increases Sirt3 levels [85]. Beyond nicotinamide, an endogenous regulator, some sirtuins inhibitors have been discovered. The most known are sirtinol and splitomicins, however both lack potent inhibitory activation of human sirtuins [84].

3.3 Mitochondrial Sirtuins

As mentioned above, each mammalian sirtuins has a distinct subcellular localization. Sirt 1, 6 and 7 are nuclear proteins and Sirt 2 is predominantly cytosolic, but it can be found in the nucleus. Sirtuin 3, 4 and 5 are present in mitochondria, more specifically in matrix [76]. In mitochondria, around 130 proteins involved in different metabolic pathways hold lysine residues that can be acetylated. Thus, the three mitochondrial sirtuins can deacetylate several proteins, regulating metabolic pathways [86]. Once Sirt3 is the most abundant of mitochondrial sirtuins, we will focus in this sirtuin.

3.3.1 Sirtuin 3

Sirtuin 3 is ubiquitously expressed in different tissues and organs [76]. Sirt3 is encoded by nuclear DNA and contains a mitochondrial targeting sequence [87]. Sirt3 has 2

different isoforms. The full-length Sirt3 (44 kDa) is present in the nucleus, where is capable of deacetylating histones such as H3 and H4. In order for Sirt3 (28 kDa) achieve its maximal activity, the full length Sirt3 undergoes a proteolytic process, after reaching mitochondria. In this process, 142 amino acids of the N-terminal segment are removed by the mitochondrial processing peptidase [88]. Although under normal situations Sirt3 is present in both nucleus and mitochondria, while under stress conditions the nuclear pool moves to mitochondria [89]. By using a mitochondrial KO model Lombard et al. (2007) showed that Sirt3 is the major mitochondrial deacetylase [90]. Indeed, Sirt3 modulates several mitochondrial pathways via deacetylation of lysine-residue, having a role in mitochondrial bioenergetics, apoptosis and cell signaling [78]. Sirt3 is directly or indirectly involved in metabolic pathways including lipid metabolism, caloric restriction conditions/insulin uptake, urea cycle, glycolysis, gluconeogenesis and TCA cycle. However, the extent of the involvement in most of the pathways is not yet well understood [81].

3.3.1.1 Regulation of Mitochondrial Metabolism by Sirt3

Sirt3 has been suggested to promote the efficient utilization of fatty acids in skeletal muscle, since it deacetylates and activates long-chain acyl-CoA dehydrogenase (LCAD), a key enzyme involved in the β-oxidation [91]. In response to exercise and lack of nutrients, Palacios et al. showed that Sirt3 may increase fatty acid utilization, because the AMP-activated protein kinase (AMPK) and Peroxisome proliferator-activated receptor-gamma coactivator 1 alpha (PGC-1α) mRNA levels are reduced in $Sirt3^{-/-}$ skeletal muscle [92].

Under ketogenic conditions, such as caloric restriction, Sirt3 regulates the production of ketone bodies. Two important enzymes in this process, acetyl-CoA Synthase 2 (AceCS2) and hydroxyl-3-methylglutaryl-CoA Synthase (HMGCS2), are deacetylated and activated by Sirt3, increasing the rate of ketogenesis [93]. Sirt3 also regulates the urea cycle, that the second enzyme involved in the mitochondrial steps of the urea cycle, ornithine transcarbamoylase (OTC) is deacetylated [82]. By using fasted mice lacking Sirt3, alterations in β-oxidation and in the urea cycle were shown, demonstrating a direct role of Sirt3 in the regulation of the two important metabolic

pathways during caloric restriction [94]. During fasting-dependent hepatic glucose production form amino acids, Sirt3 deacetylates and activates glutamate dehydrogenase (GDH), an enzyme responsible for the conversion of glutamate into the tricarboxylic acid cycle intermediate α-ketoglutarate [95]. Sirt3 also activates isocitrate dehydrogenase 2 (IDH2), increasing NADH production [82]. In addition, Sirt3 deacetylates and decreases the activity of cyclophilin D (Cyp D), promoting the dissociation of hexokinase II from the OMM, reducing glycolysis [96]. Sirt3 can also deacetylate oxidative phosphorylation complexes, more specifically complex I, II and III subunits [78, 97]. Studies demonstrated that mitochondria from Sirt3$^{-/-}$ animals display a selective inhibition of complex I activity and decreased basal ATP content [98]. By performing a proteomic study, Law et al. (2009) showed that Sirt3 binds to ATP synthase as well [99]. In mitochondria, Sirt3 can also regulate protein translation by deacetylating the mitochondrial ribosomal protein L10 [82]. All the above mentioned data suggest that Sirt3 has an important impact in metabolic control and support mitochondrial oxidation and ATP production under basal conditions. Indeed Sirt3$^{-/-}$ mice exhibit reduction in basal ATP in several tissues [100].

3.3.1.2 Regulation of other pathways by Sirt3

Along with histones, also many transcription factors, such as p53 and NFκB were identified as targets for deacetylation, determining the ability of cells to adapt to different conditions [82]. Sirt3 has a role in signaling, acting in signaling molecules such as ROS or NO [78]. Sirt3 modulates ROS, up-regulating SOD II expression and indirectly increases the activity of others ROS-detoxifying enzymes [101]. When Sirt3 deacetylates IDH2 and GDH both enzymes increase the production of NADPH, which is required for glutathione reductase to convert oxidized to reduced glutathione. It is a cofactor for mitochondrial glutathione peroxidase in its ROS scavenging activity [95]. Shinmura et al. (2011), supported this idea by demonstrating that an activator of Sirt3 (resveratrol) decreased ROS production and improved cell survival after hypoxia/reoxygenation [102]. Mitochondrial aldehyde dehydrogenase 2 (ALDH2) is

also a Sirt3 target, and its activity leads to the removal of aldehydes, which are accumulated in hearts due to excessive ROS [103].

Sirt3 can likewise regulate cell death and survival, being the pro-apoptotic or anti-apoptotic activity dependent of cell type [104]. In Hela cells, Sirt3 deacetylates Ku70, a protein present in the ku protein complex, involved in DNA damage repair. Ku70 deacetylation promotes Ku70/Bax interaction and blocks the translocation of Bax to mitochondria, increasing cell resistance to Bax-mediated cell damage [101]. Under stress conditions, increased expression of Sirt3 protects cardiomyocytes, due in part by hindering the translocation of Bax to mitochondria [105]. CyP D, a MPT pore regulator, interacts with Sirt3 and is inactivated, elevating the threshold for pore opening, de-sensitizing it to cellular stress [96]. AMPK is regulated by the cellular energy changes, regulating ATP production and serving as a key regulator of cell survival. In cardiomyocytes, Sirt3 can activate serine-threonine liver kinase B1 (LKB1), which subsequently promote AMPK phosphorylation that can inactivate GSK3β and upregulate GLUT4 protein, protecting cardiomyocytes from hypertrophy [106]. On the other hand, Sirt3 plays a pro-apoptotic role in both Bcl-2/p53 and JNK-regulated apoptosis. Kim et al. (2010) work supports the pro-apoptotic role, showing that cells lacking Sirt3 have decreased stress-induced apoptosis [107]. This dual role is still unclear and needs more investigation to understand the mechanisms and different pathways involved.

Objectives

The main objective of the study was to understand the role of Sirt3 on H9c2 cardiomyoblasts treated with DOX, more precisely whether Sirt3 protects H9c2 cells against DOX-induced cardiotoxicity.

In order to test this hypothesis, the first aim was the production of Sirt3 Knock-down and overexpressing H9c2 cardiomyoblasts. The second aim was to compare the DOX toxicity on naïve and Sirt3 KD/overexpressing cardiomyoblasts, thus concluding on the role of that mitochondrial sirtuins on anthracycline toxicity.

Chapter 2 – Material and Methods

1. Reagents

Dulbecco's modified Eagle's medium (DMEM), fetal bovine serum (FBS), Penicillin-Streptomycin, 0.05% Trypsin-EDTA, 1x Opti-MEM Reduced Serum Medium were received from Invitrogen (Carlsbad, CA, USA). Doxorubicin, Sulforhodamine B (SRB), protease inhibitor cocktail (PMSF), bovine serum albumin (BSA), ammonium persulfate (APS), Bradford reagent, calcium chloride ($CaCl_2$), ethylenediaminetetraacetic acid (EDTA), β-mercaptoethanol, sodium dodecyl sulfate (SDS) and trypan-blue were obtained from Sigma-Aldrich (St. Louis, MO, USA). Other chemical reagents were also purchased from Sigma-Aldrich, including those necessary to prepare 1x Phosphate Buffered Saline (PBS) (0.137 –m NaCl, 2.7 mM KCl, 1.4 mM KH_2PO_4, 0.01 M Na_2HPO_4). Cell Lysis Buffer were obtained from Cell Signaling (Danvers, MA, USA). Acrylamide, Laemmli buffer, Polyvinylidene Difluoride membrane (PVDF) membranes and N,N,N',N'-Tetramethyllenediamine (TEMED) were from BioRad (Hercules, CA, USA). The ECF detection system was obtained from Healthcare Life Sciences (Buckinghamshire, UK). Acetic acid and ethanol were obtained from Merck (Whitehouse Station, NJ, USA)

All reagents and chemical compounds used were the greatest degree pf purity commercially available. In the preparation of every solution, ultrapure distilled water filtered by the Milli Q from Millipore system was always used.

2. Cell model

H9c2 cell line was isolated initially by Kimes and Brandt. This cell line is a subclone of the original and is derived from embryonic BD1X rat heart tissue. According to Kimes and Brandt, H9c2 propagates as a mononucleated myoblats and exhibits electrophysiological and biochemical properties of both skeletal and cardiac muscle [108, 109]. The mono-nucleated myoblasts can differentiate and acquire skeletal muscle phenotype, under reduced serum concentration. On the other hand, treatment with retinoic acid prevents the differentiation into skeletal muscle and favors the establishment of cardiac phenotype (Fig. 2) [110]. The H9c2 cardiomyoblasts cell line is

considered an excellent model for cardiac cells. H9c2 cell line (ATCC® Number: CRL-1446TM) was purchased to American Type Cell Culture (ATCC®, Manassas, VA).

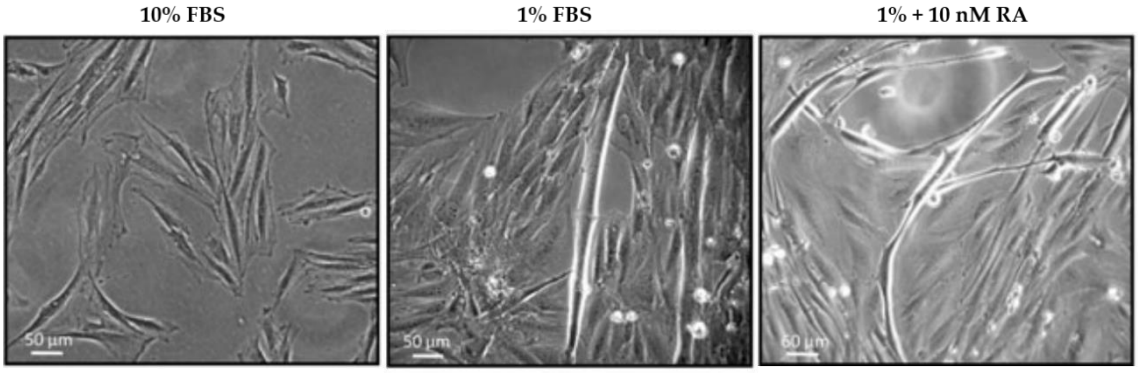

Figure 2 – Differentiation of H9c2 cell line: The condition with 10% FBS shows typical morphology of undifferentiated cells characterized by mononucleated and small spindle shaped myoblasts. During differentiation, the reduction of serum to 1% leads to multinucleated long skeletal muscle myotubes, while addition of 10 nM of retinoic acid leads to the generation of multinucleated cardiomyocytes. Images courtesy from Dr. Vilma Sardão [110].

3. Cell Culture

The cells were grown in Dulbecco's Modified Eagle Medium (DMEM) supplemented with 10% FBS, 1.5g/L sodium bicarbonate and 1% of penicillin-streptomycin in 60 or 100 mm cell culture dishes at 37ºC in a humidified atmosphere of 5% CO_2. The cells were fed every 2 - 3 days and sub-cultured once they reached approximately 80% confluence in order to prevent cell differentiation. For this routine process, cells were first rinsed with PBS 1x and then incubated with 1 volume of Trypsin-EDTA for 3 min at 37ºC. Trypsin activity was inhibited by the addition of 1 volume of growth medium and then centrifuged 3 min. Cells were resuspended and seeded again. Cells were used between passages 7 and 20.

4. Transformation of Competent Cells and Plasmid Purification

One Shot® TOP10 Chemically Competent E.coli (Invitrogen™) was used to transform cells, for high-efficiency cloning and plasmid propagation, according to the manufacturer's protocol. The plasmids were provided by Dr. Michael Sack (National Heart, Lung and Blood Institute, National Institutes of Health). Following transformation procedure, cells were harvested by centrifugation at 6000g for 15 min at

4ºC and the pellet was saved. After, plasmid purification was performed using Hispeed Plasmid Midi Kit (Quiagen, Valencia, CA) by following the manufacturer's protocol. The DNA concentration was determined with a Nanodrop spectrophotometer (Thermo Scientific, Lanham, MD). The purity of the sample was examined through the 260/280 and 260/230 ratio, being a sample considered contaminated when the ratios were different than 2.

5. Sirt3 Gene Overexpression in H9c2 cells

To evaluate the role of Sirt3 in H9c2 cardiomyoblats, the wild-type (hSirt3-Flag), the constructs without catalytic activity (hSirt3-H248Y-HA) and the empty vector (PcDNA), all obtained with the above procedure, were overexpressed in these cells. In order to form the complexes of DNA, a 1:3 ratio of 9μg of DNA and 27μl of X-tremeGENE HP DNA Transfection Reagent (Roche, Mannheim, Germany) was used in Opti-MEM I Reduced Serum Medium, for 15 minutes. Afterwards, the transfection was performed and cells were incubated in growth medium for 24h, to obtained a transiently protein transfection. Besides the three groups described above, one control condition was performed using only transfection reagent.

6. Sirt3 Gene Underexpression in H9c2 cells

Sirt3 silencing was performed using a small interfering RNA (siRNA). Cells were transfected with 3 μg of Sirt3 siRNA oligonucleotide (Target sequence: GCUCAUGGGUCCUUUGUAU, GGAUGGACAGGACGGAUAA, CAGCAAGGUUCUUACUACA and CAGCUUGUCUGAAUCGGUA) or scrambled siRNA (Thermo Fisher Scientific), which functions as empty vector. Transfection was performed using Xtreme gene siRNA transfection reagent (Roche, Mannheim, Germany), according to the manufacturer's instructions. Before transfection, the medium of the plates was changed from DMEM to Opti-MEM (3 ml) and for each dish, 18 μl of Xtreme were added to 100 μl of Opti-MEM, in a centrifuge tube. After, 12 μl of siRNA were diluted in 100 μl of Opti-MEM, on another centrifuge tube, to obtain the

desired concentration of 3 μg. Next, the content of both tubes was combined and incubated for 15 min at room temperature allowing complexes to form. Once the incubation was complete, 200 μl of complexes was added to dishes containing cells and after 5 hours of incubation in Opti-MEM, 9 ml DMEM was added. Similarly to overexpression experiments, a control condition was prepared with transfection reagent.

7. Experimental Design

The experimental design is shown in Fig. 3. For qRT-PCR and WB, H9c2 cells were plated at a density of 50,000 for control and 85,000 cells/ml for the other conditions in 60 mm culture dishes and cultures for one day. Then, cells were transfected and 24h afterwards were treated with DOX. Two concentrations were used, 0.5 and 1μM, which was directly added to culture media and 24 hours post-treatment, cells were collected and stored at -80ºC (Fig. 3A).

For the others assays, such as SRB, flow cytometry and fluorescence microscopy, cells were seeded in order to reach a density of 60 -70% in next day, to be transfected. Twenty-four hours after transfection, cell seeding was performed at a density of 10,000 cells/ml in 48 a multi-well for SRB; 20,000 cells/ml in 6 multi-well with 18x18mm coverslip for microscopy and 40,000 cells/ml in 6 multi-well for flow cytometry. The following day, DOX was added as described before and 24h afterwards cells were used to the assays (Fig. 3B).

Previous studies in our lab showed no differences in SRB between the two designa used. Viable cell counting was performed by using Trypan Blue.

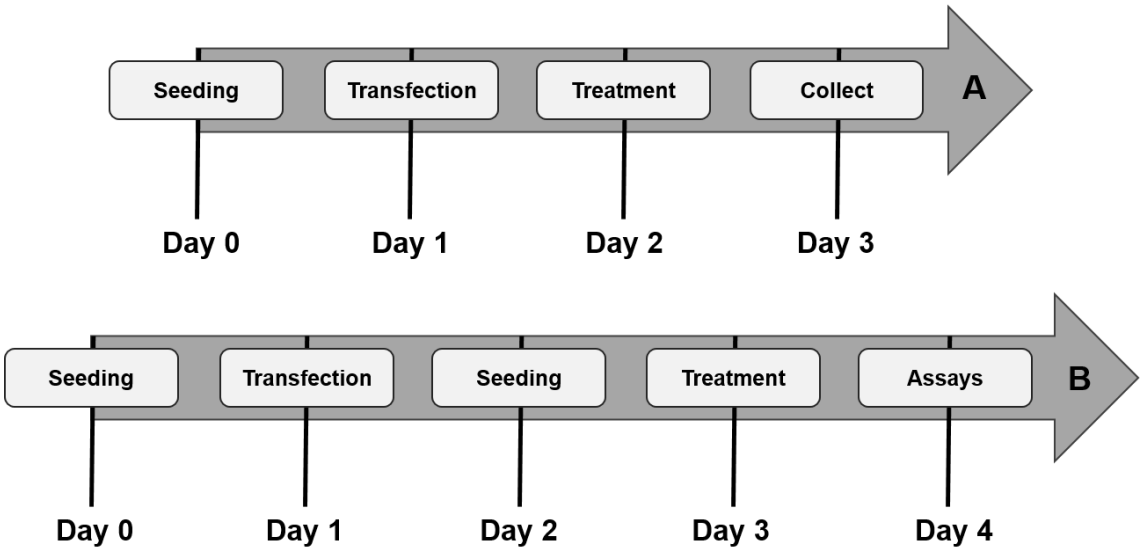

Figure 3– Experimental design: A) For Western Blot and RT-PCR experiments. B) For the other set of experiments, such as SRB, flow cytometer and fluorescence microscopy.

8. Sulforhodamine B Colorimetric Assay

Cell mass was measured using SRB dye, which measures the total biomass by staining cellular proteins. After treatment, the incubation media were removed, and cells were washed twice with PBS and fixed in ice cold methanol containing 1% acetic acid overnight at -20ºC. Multi-well plate containing fixed cells was then dried at 37ºC and 250 µl of 0.5% SRB in 1% acetic acid was added to each well and incubated for 1 hour at 37ºC. Subsequently, SRB was removed and wells were washed with 1% acetic acid to removed unbound staining. After drying the plates again, dye bound to cells proteins was extracted with 10 mM Tris base solution (pH 10) and its absorbance was read at 540 nm in a VICTOR X3 Microplate Reader (Perkin Elmer, Waltham, MA, USA).

9. Western-Blot Analysis

9.1 Total Protein Harvesting

On collection day, cells grown in 60 mm culture dishes were washed once with 1x PBS, detached with 1 volume of trypsin-EDTA followed by its inactivation with 1 volume of growth medium, previously removed from the dish and stored. Cells were transferred to a 15 ml conical tubes and centrifuged, supernatant was discarded and pellet rinsed

in 1x PBS. Cells were centrifuged under the same conditions, the supernatant was discarded again and the pellet was stored at -80ºC. Before protein quantification, 100 µl of cell lysis buffer with PMSF, a protease inhibitor, was added to each pellet and samples were then sonicated.

9.2 Protein Quantification

Protein was quantified using the Bradford assay. The samples were diluted 1:400 in ultrapure water and 1000 µl of Bradford reagent was added to the samples. Then, 200 µl of the each mix were plated in 96 multi-well plate and after 15 min of incubation at 37ºC, absorbance was read in VICTOR X3 Microplate Reader at 595 nm. The standard curve ranging from 1.25 to 20 µg/ml was made using a known concentration of solution of Bovine Serum Albumin (BSA).

9.3 Western Blot

After denaturation at 95ºC for 5 min in a 2x *Laemmli* sample loading buffer (Bio-Rad), an equivalent amount of protein (40µg) was separated by 10% polyacrylamide gel electrophoresis system. Protein separation was carried out at a constant voltage of 150 V and at room temperature. In every gel, a molecular weight standard (Precision Plus Protein Standards – Dual Color, Bio-Rad) was included to allow molecular weight estimation. Once protein separation was complete, proteins were transferred to a PVDF (Millipore), during 90 min at a constant voltage (100 V). In order to mitigate the heat produced during the transference, ice was incorporated in the outside. After membrane blocking with 5% milk (Bio-Rad) in Tris-Buffered Saline Tween (TBS-T; 50 mM Tris-HCl, pH 8; 154 mM NaCl NaCl and 0.1% Tween 20) for 2 hours at room temperature under continuous stirring, membranes were washed 3 times for 5 min each with TBS-T. An incubation with a primary antibody directed against the respective protein was the performed (listed in Table 1) overnight at 4ºC, under continuous stirring. All primary antibodies were prepared in 2% milk in TBS-T supplemented with sodium azide. Once incubation was complete, membranes were washed 3 times for 5 min with TBS-T and were further incubated with alkaline

phosphatase conjugated secondary antibodies for 1 hour at room temperature under continuous agitation. All secondary antibodies were prepared in TBS-T (1:2,500). Finally, membranes were washed again and incubated with Enhanced Chemi-Fluorescence system (ECF) (GE Healthcare), maximum for 5 min at room temperature. Fluorescence was read using the UVP Biospectrum 500 Imaging System (UVP LLC, Cambridge, UK) through UV epi-ilumination (365 nm). Densities of each band were calculated with VisionWorksLs Analysis Software. Before blocking, the membranes were stained with Ponceau S reagent to confirm equal protein loading in each membrane [111].

Name	*Dilution*	*Host Species*	*MW (kDa)*	*Catalog Number*	*Manufacturer*
Acetyl-p53	1:500	Rabbit	53	06-758	Millipore
Caspase 3	1:1000	Rabbit	17/35	9662	Cell Signaling
Caspase 8	1:1000	Rabbit	10/57	4790	Cell Signaling
Caspase 9	1:750	Rabbit	25/35-37/45	Ab25758	Abcam
OXPHOS	1:1000	Mouse	20/30/47/39/53	MS 604	MitoSciences
p53	1:1000	Mouse	53	2524	Cell Signaling
Sirt3	1:1000	Rabbit	28	2627	Cell Signaling
SOD II	1:750	Rabbit	25	ab13533	Abcam

Table 1: List of primary antibodies used in Western Blot protein analysis. Relatively to caspase 3, the lower molecular weight corresponds to the large fragment resulting from cleavage and the other value to full length caspase 3; for caspase 8, the antibody detects the total caspase 8 (57kDa) and the p10 subunit of the activated protein. Caspase 9 antibody identifies 45 kDa pro-caspase 9, 35-37 kDa cleaved large fragment and the 25 kDa fully cleaved caspase 9. The OXPHOS Antibody Cocktail contains 5 different antibodies: complex I subunit NDUFB8 (20 kDa), complex II SDHB (30kDa), complex III subunit UQCRC2 (47 kDa), complex IV MTCO1 (39 kDA) and complex V subunit ATP5A (53 kDa).

10. Evaluation of Cell Death by Flow Cytometer

To evaluate cell death, transfected cells were harvested by trypsin and resuspended in buffer medium (120mM NaCl, 3.5mM KCl, 0.4mM KH2PO4, 20mM HEPES, 5mM

NaHCO3, 1.2mM NaSO4, 10mM sodium pyruvate at pH 7.4) supplemented with 1.2mM MgCl2, 1.3mM CaCl2. Next, a set of cells were incubated with 100 nM Sytox Green and the other with 800 nM Calcein-AM. These probes give us information about dead and live cells, respectively. Two samples of non-labeled cells, with and without DOX, were also analyzed in order to calibrate the system, taking cell self-fluorescence and DOX fluorescence into account. Samples were kept on ice until use and 8,000 cells were analyzed on a FACSCalibur Flow Cytometer (BD Biosciences, San Jose, California, USA). Data was analyzed using CellQuest Pro Software Package.

11. Fluorescence Microscopy

To perform this experiment, cells were plated on coverslips in 6 multi-well plate as described above. On the day of the assay, cells were rinsed with PBS and incubated in buffer medium (already described in 10.) with different probes, for 30 minutes. After incubation, coverslips were removed from the wells and placed inverted on slides. All images were obtained with Nikon Eclipse Ti-S (Nikon Instruments Inc., NY, USA). Mitochondrial transmembrane potential alterations were analyzed by co-labeling cells with TMRM (100nM), which is accumulated by polarized mitochondria, and with Hoechst 33342 (1μg/ml) that counterstain the nucleus. Oxidative stress was also evaluated by fluorescent microscopy, using MitoSox Red (5μM) in the presence of the mitochondrial probe MitoTracker Green (200 nm). The probe MitoSox Red is specifically accumulated in mitochondrial matrix and allows the identification of superoxide anion generated in mitochondria, while MitoTracker Green stains mitochondria, independently of membrane potential. Rotenone (250 μM), complex I inhibitor, was used as a positive control of superoxide anion generation.

12. Quantitative RT-PCR Analysis

12.1 Total RNA Harvesting

In the day of the harvesting, cells grown in 60 mm dishes were collected as described before and rinsed twice with 1x PBS. After pellets were saved at -80ºC until the day of RNA extraction. Total RNA was isolated using the Total RNA Mini Kit (Bio-Rad),

according to the manufacturer's protocol. On the last step, RNA was eluted twice from the columns with 40 µl RNA elution solution to a new centrifuge tube, Then RNA was quantified using a NanoDrop spectrophotometer (Thermo Fisher Scientific) to measure the absorbance at 260 nm. The RNA quality and purity was tested by spectral scan observation and considered when a single prominent 260 peak and a 260/280 ratio with a minimum value of 2 was found.

12.2 Evaluation of RNA integrity

RNA integrity and purity was analyzed using the Experion RNA Analysis Kits (Bio-Rad). For the procedure, 12 random samples were evaluated according to manufacturer's protocol by Experion Automated Electrophoresis System (Bio-Rad, CA, USA). RNA quality indicator (RQI) a number automatically generated by the program, on a scale of 1-10, was analyzed and if RQI was from 7 to 10, the RNA sample was used in the next step.

12.3 Reverse Transcription PCR

The first step involves the reverse transcription of total mRNA into cDNA using the iScript cDNA Synthesis Kit (Bio-Rad). The kit contained a reverse transcriptase enzyme and a mix with oligo(dT) and random hexamer primers, which optimizes the sensitivity and extension of the reverse transcription reaction. The iScript mix was diluted in nuclease-free water and 1 µg of Total RNA to a final volume of 20µl. The solution was loaded in PCR strips tubes and the reactions were performed in a Bio-Rad S1000 Thermal Cycler. The reaction protocol was: 5 min at 25ºC, 30 min at 42ºC and 5 min at 85ºC.

12.4 Real Time PCR

mRNA transcript levels were quantified in real-time PCR using SsoFast EvaGreen Supermix (Bio-Rad). One µl of cDNA samples and 100 µM of genetic-specific forward and reverse primers in 20 µl total reaction volume was used. Amplification and

quantification of generated products were performed in a CFX96 Real-time PCR detection system (Bio-Rad) under the following cycling conditions: a single step of 95ºC for 30 sec, 40 cycles of 95ºC for 5 sec followed by another 5 sec at 60ºC with single-point fluorescence acquisition at the end. Finally, a melting curve was performed to confirm that only the expected products were generated. Samples were run in duplicates and with a standard curve. Moreover, a non-template control (NTC) and a negative control without cDNA template (NRT) were also included to exclude contamination. None of the runs showed expression on these conditions. All reactions were normalized using 18S as a reference gene.

After obtaining nucleotide accession numbers from the database, all primers were designed using the Primer-Basic Local Alignment Search Tool (Primer-Blast). Primers are listed in table 2.

Name	***Sequence***	***Amplicon (bp)***	***T (ºC)***
Sirt1	F – CCAGTAGCACTAATTCCAAGTTCT R – CTCGCCACCTAACCTATGAC	150	62
Sirt3	F – CCAATGTCGCTCACTACTT R – GATACCAGATGCTCTCTCAAG	101	63
Sirt4	F – CTGCTAAAGACCCCTAAG R – GCCCTCATCTCTGTAAATAG	136	63
Sirt5	F – GCTCGTCCAAGTTCCAATATG R – CCACTCTCCGCACTAACA	98	63
GADD45	F – CTGGTGACGAACCCACATTC R – CCACTGATCCATGTAGCGACTT	93	60
TBP	F – CCTATCACTCCTGCCACACC R – CAGCAAACCGCTTGGGATTA	154	62
18S	F – ACTCAACACGGGAAACCTC R – ACCAGACAAATCGCTCCAC	122	63

Table 2: List of primers used in RT-PCR analysis. Amplicon (bp): Amplicon in base pairs; T (ºC): Annealing temperature in Celsius.

13. Statistical Analysis

Statistical analysis was performed with GraphPad Prism 6 and data are presented as Means ± SEM. To evaluate the effect of two variables, namely transfection effect and treatment, a two-way ANOVA followed by the Tukey Multiple Comparison Test was applied. To compare the effect of DOX in control cells, a one-way ANOVA followed by the Tukey post-test was used. A *p* value of <0.05 was considered significant ($p < 0.05$, $pp < 0.01$, $ppp < 0.001$).

Chapter 3 – Results

1. Sirt3 gene and protein expression in H9c2 cells

Sirt3 protein content in H9c2 cells was analyzed by Western blotting. Using a commercial antibody, a reduced endogenous Sirt3 protein content was detected, both the short (28 kDa) as long (44kDa) forms (Fig. 4A and 5A). Sirt3 gene expression was also quantified using real-time PCR and similarly to in WB a very low endogenous quantity was identified in H9c2 wild-type cells. In underexpression control conditions Sirt3 short-form increased with both DOX concentrations (Fig. 5B) and in the overexpression model, a significant increase was measured between 0.5 and 1 μM of DOX, with Sirt3 long-form not showing a significant alteration (Fig. 4B and 4D). The Sirt3 overexpression was obtained through the use of Sirt3 wild-type plasmid (hSirt3) and deacetylase catalytically inactive construct (hSirt3 mutant). An empty vector was used as a control (PcDNA). hSirt3 and hSirt3 mutant overexpression lead to a large increase of both forms of Sirt3 expression, for all three groups, indicating an efficient transfection. Without DOX, hSirt3 mutant showed a significant increase of Sirt3 protein content comparing with hSirt3 (Fig. 4C e 4E). During Sirt3 underexpression (sSirt3), an increase of Sirt3 protein with empty vector (EV) transfection and 1μM of DOX was evident. Only in 1 μM DOX condition a significant reduction of Sirt3 protein content was detected (Fig. 5C).

Curiously, Sirt3 mRNA levels decreased in control cells and overexpressed Sirt3 control cells with 1 μM of DOX. Without DOX, hSirt3 mutant and hSirt3 overexpressing cells showed an increase in Sirt3 mRNA, although only in hSirt3 overexpression the increase was significant. hSirt3 overexpression cells also showed an increase of Sirt3 mRNA levels when treated with 1 μM DOX (Fig. 6A and 6B). RT-PCR was also performed to analyze the underexpression model. This experiment was realized without DOX and only one time. In sSirt3 underexpression cells, Sirt3 mRNA levels decreased about 50% (Fig. 6C).

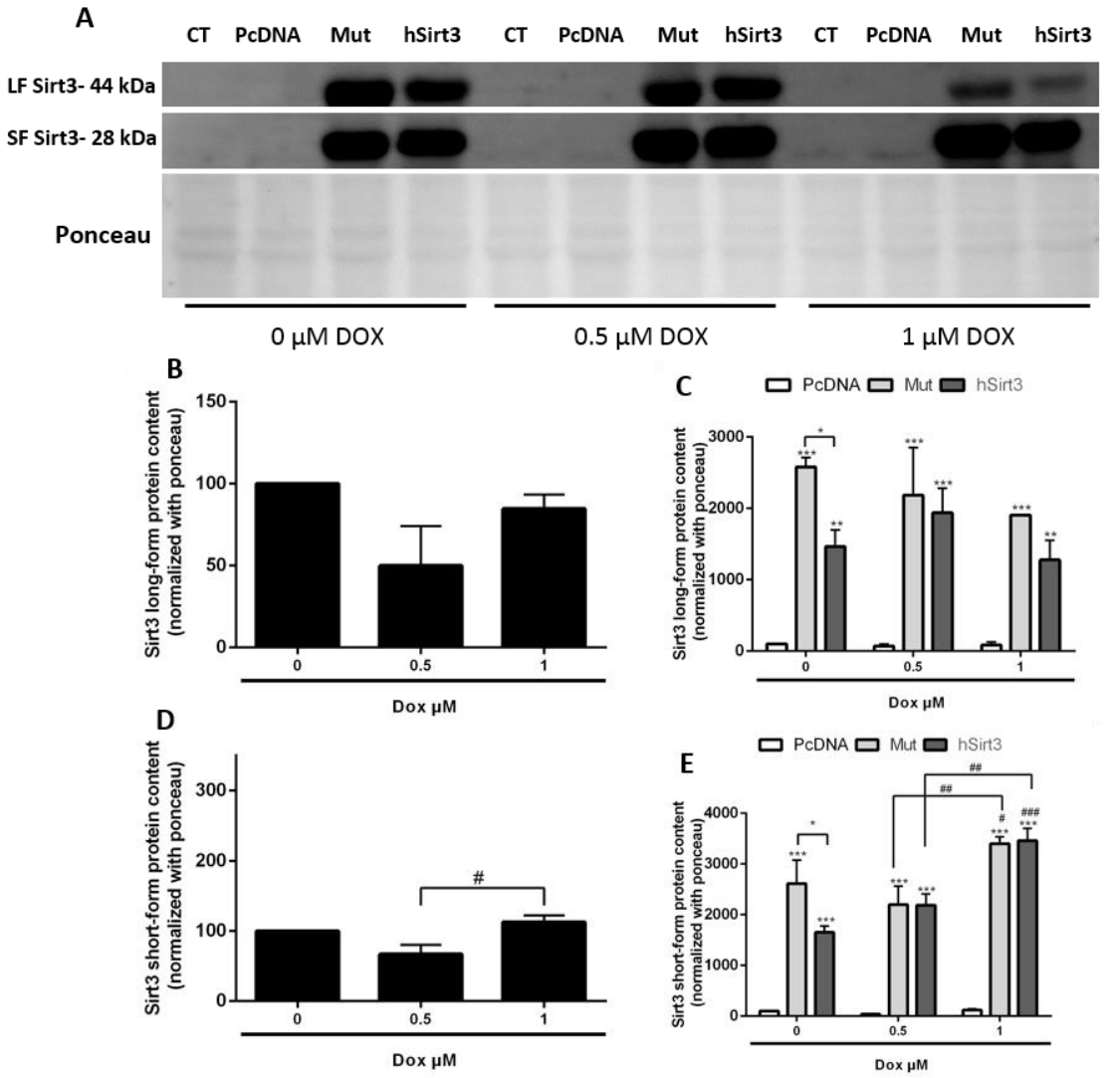

Figure 4 – Endogenous Sirt3 protein and Sirt3 overexpression in H9c2: The western blot to analyze Sirt3 protein content was performed after transfection and treatment with DOX. A) Representative western blot of Sirt3: Sirt3 short-form (28 kDa) and Sirt3 long-form (44 kDa). B and D) Control cardiomyoblasts cells with transfection reagent. Results are normalized to the control without DOX. C and E) Overexpression experiment using empty vector cells as control (PcDNA), Sirt3 deacetylase mutant cells (Mut) and Sirt3 overexpression cells (hSirt3). Results are normalized to the control, no DOX, transfected cells. Data represents Mean ± SEM of 3 – 4 independent experiments. Statistical analysis was performed by using one-way ANOVA for B and D or two-way ANOVA for C and E. # Analysis made inside the same transfection condition. * vs control of the same concentration of DOX. One symbol= $p< 0.05$, two symbols= $p< 0.01$ and three symbols= $p<0.001$.

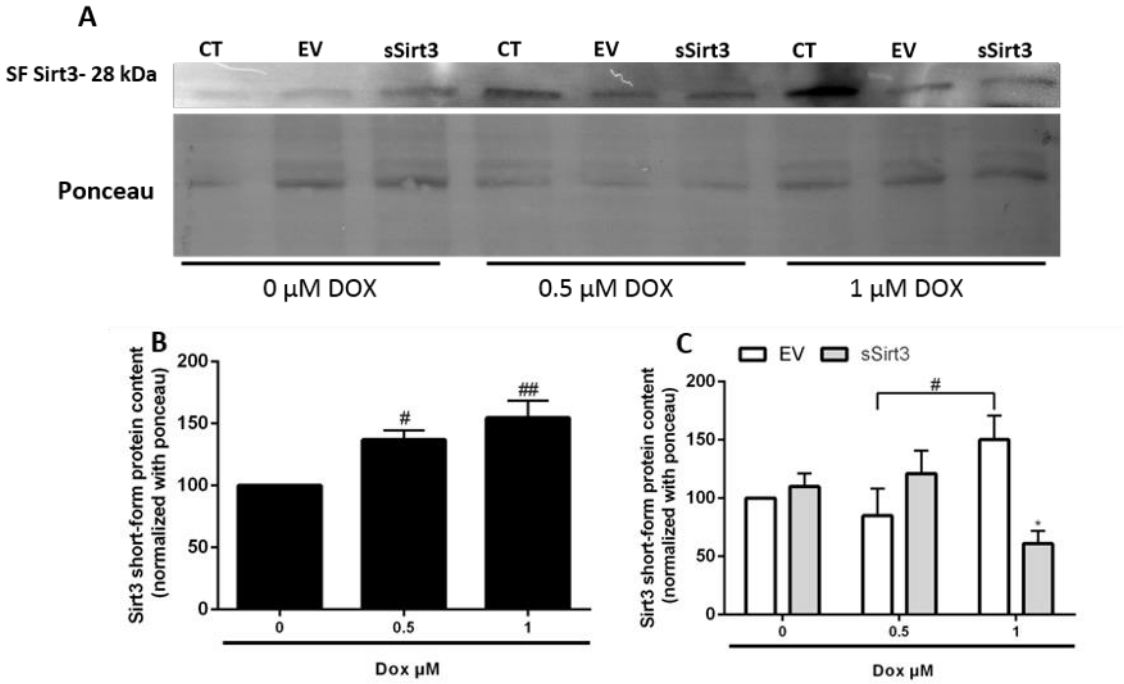

Figure 5– Sirt3 endogenous and underexpression protein content in H9c2 cells: A) Representative western blot of Sirt3 short-form (28 kDa). B) Control cardiomyoblasts with transfection reagent and DOX. Results are normalized to the control without DOX. C) Underexpression experiment using empty vector cells as control (EV) and Sirt3 silenced cells (sSirt3). Results are normalized to the control, no DOX, transfected cells. Data represents Mean ± SEM of 3 – 4 independent experiments. Statistical analysis was performed by using one-way ANOVA (B) and two-way ANOVA (C). # Analysis made inside the same transfection condition. * vs control of the same concentration of DOX. One symbol= p< 0.05, two symbols= p< 0.01 and three symbols= p<0.001.

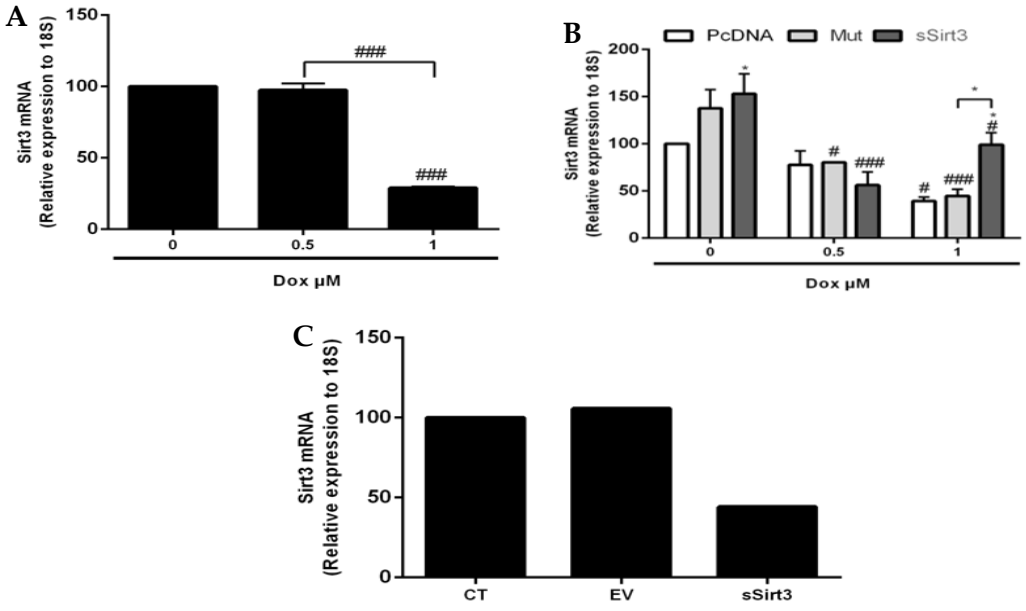

Figure 6- Sirt3 mRNA levels in H9c2 Cardiomyoblasts: Sirt3 mRNA levels were quantified by RT-PCR in control cells with and without DOX (A) and in control PcDNA, hSirt3 mutant and

hSirt3 overexpressing cells in control and DOX-treated conditions (B). Results are normalized to the control, no DOX, transfected cells. Data represents Mean ± SEM of 2-3 independent experiments. Statistical analysis was performed by using one-way ANOVA (A) and two-way ANOVA (B). # Analysis made inside the same transfection condition. * vs control of the same concentration of DOX. One symbol= p< 0.05, two symbols= p< 0.01 and three symbols= p<0.001. C) RT-PCR performed in control, control EV transfected and sSirt3 cells without DOX. Data represents 1 independent experiment.

2. Sirt3 does not protect against DOX-induced decreased H9c2 cell mass

H9c2 cell mass was determined by the SRB assay, after Sirt3 manipulation and 24h of incubation with 0.5 and 1 μM of DOX. This method does not differentiate between DOX-induced inhibition of cell proliferation and induction of cell death. Both DOX concentrations induced a significant decrease of H9c2 cardiomyoblast mass (Fig. 7A and 7B). The results also showed that neither overexpression nor underexpression of Sirt3 altered the decrease in cell mass caused by DOX treatment (Fig. 7C and 7D).

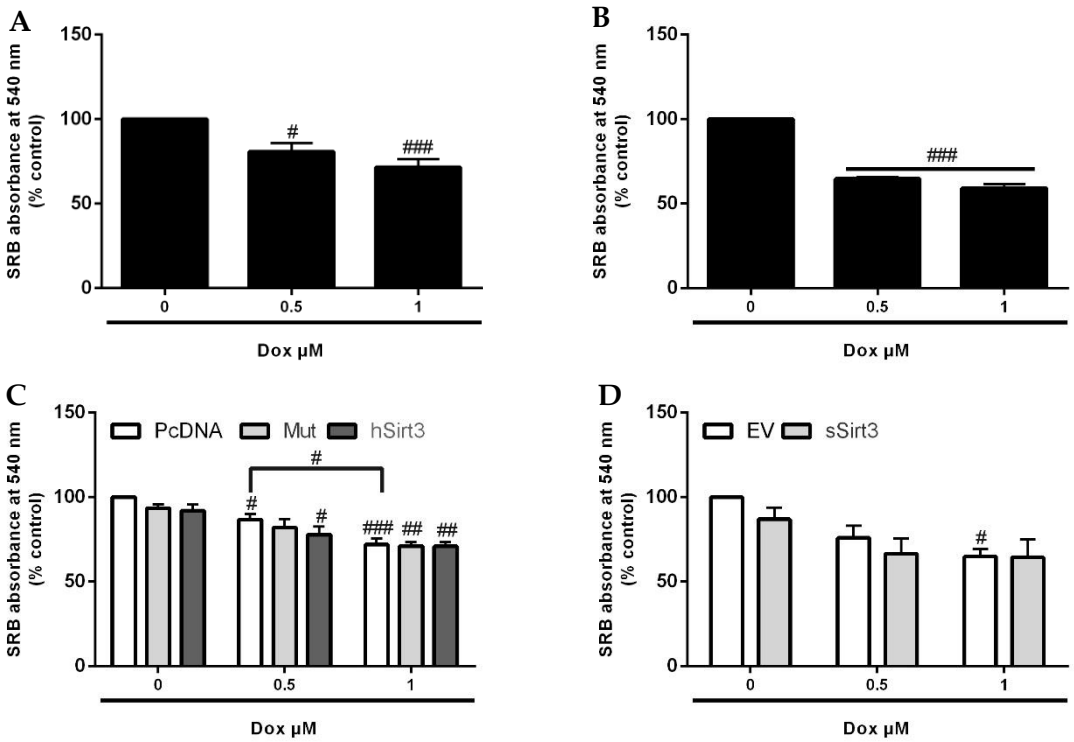

Figure 7– Sirt3 does not protect against DOX-induced decreased cell mass: The experiment was performed 24 hours after DOX treatment in all conditions. A and B) Overexpression and underexpression control cells with transfection reagent, respectively. Results are normalized to

the control without DOX. C) Overexpression experiment using empty vector cells as control (PcDNA), Sirt3 deacetylase mutant cells (Mut) and Sirt3 overexpression cells (hSirt3). D) Underexpression assay with empty vector as control cells (EV) and Sirt3 silencing (sSirt3). Results are normalized to the control, no DOX, transfected cells. Data represents Mean ± SEM of 3 – 5 independent experiments. Statistical analysis was performed by using one-way ANOVA for A and B, and two-way ANOVA for C and D. One symbol= $p< 0.05$, two symbols= $p< 0.01$ and three symbols= $p<0.001$. # Analysis made inside the same transfection condition.

3. Sirt3 presents a small effect on DOX-induced H9c2 cell death

Using Sytox green and Calcein-AM, dead and live cells were measured respectively, by flow cytometry. A significant reduction in live cells after DOX treatment was observe in naïve H9c2 cardiomyoblasts, corroborated by the increase of dead cells. The results for dead cells after 1 μM DOX treatment also exhibited a significant difference in comparison to cells treated with 0.5 μM of DOX, which could be due to the fact that Sytox green internalize not only dead cells but those, which although are positive for calcein, present damaged membranes (Fig. 8A and 8B). In order to understand the effect of Sirt3 in DOX-induced cell death, Sirt3 overexpression was performed followed by DOX treatment. By following Sytox green fluorescence, control PcDNA transfected cells showed a decreased in dead cells with DOX. This can be explained by the great variation in cell death and vector toxicity, since our control group represents PcDNA transfected cells, which showed more cell death than control cells without the empty vector. During Sirt3 overexpression, and not during Sirt3 mutant overexpression, a significant decrease of dead cells was observed in the condition without DOX. However, this did not happen with DOX treatment. Although not statistically significant, the results regarding live cells exhibited an increasing trend following Sirt3 overexpression (Fig. 8C and 8D).

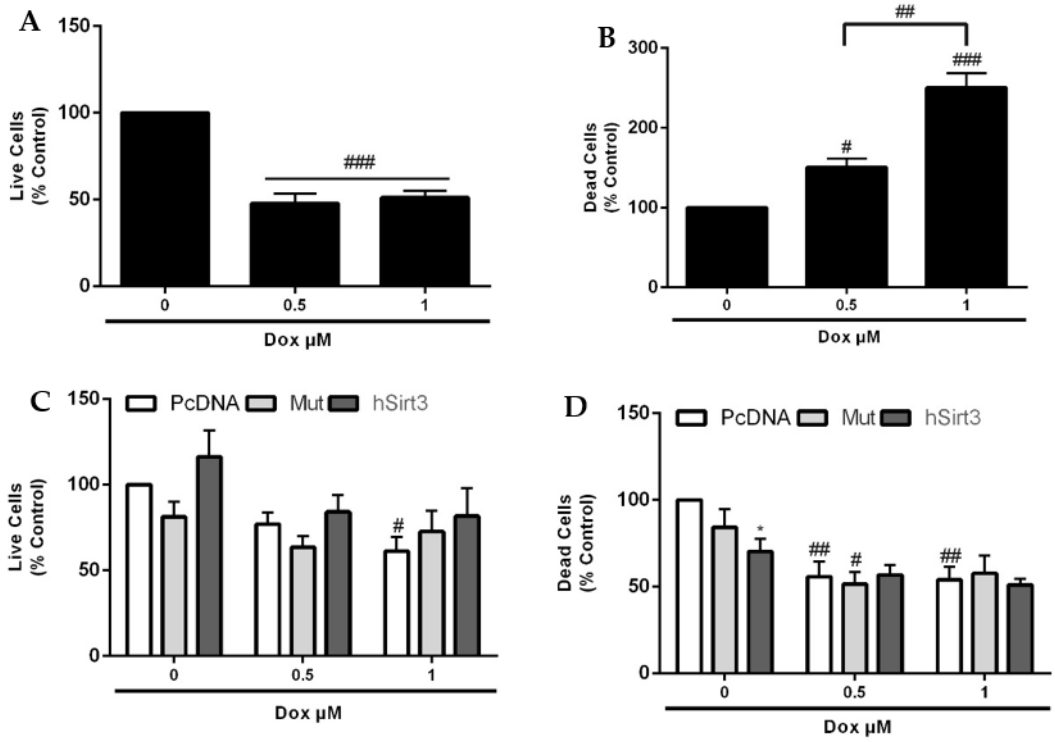

Figure 8– Sirt3 overexpression against DOX-induced cell death: The experiment was performed using flow cytometer in cells labeled with Calcein-AM to measure live cells and Sytox green to quantify dead cells. After Sirt3 overexpression assay and DOX treatment, flow cytometer was realized. A and B) Live and dead cells were measured in overexpression control cells, containing only transfection reagent. Results are normalized to the control without DOX. C and D) Overexpression experiment using empty vector cells as control (PcDNA), Sirt3 deacetylase mutant cells (Mut) and Sirt3 overexpression cells (hSirt3). Results are normalized to the control, no DOX, transfected cells. Data represents Mean ± SEM of 3 independent experiments. Statistical analysis was performed by using one-way ANOVA for A and B, and two-way ANOVA for C and D. One symbol= $p< 0.05$, two symbols= $p< 0.01$ and three symbols= $p<0.001$. # Analysis made inside the same transfection condition. * vs control of the same DOX concentration.

We also measured protein content for the initiator caspase 8 and 9, and effector caspase 3 by using western blotting. Caspase 8, a key component of the extrinsic pathway did not show any difference in any of the experimental groups tested (Fig. 9).

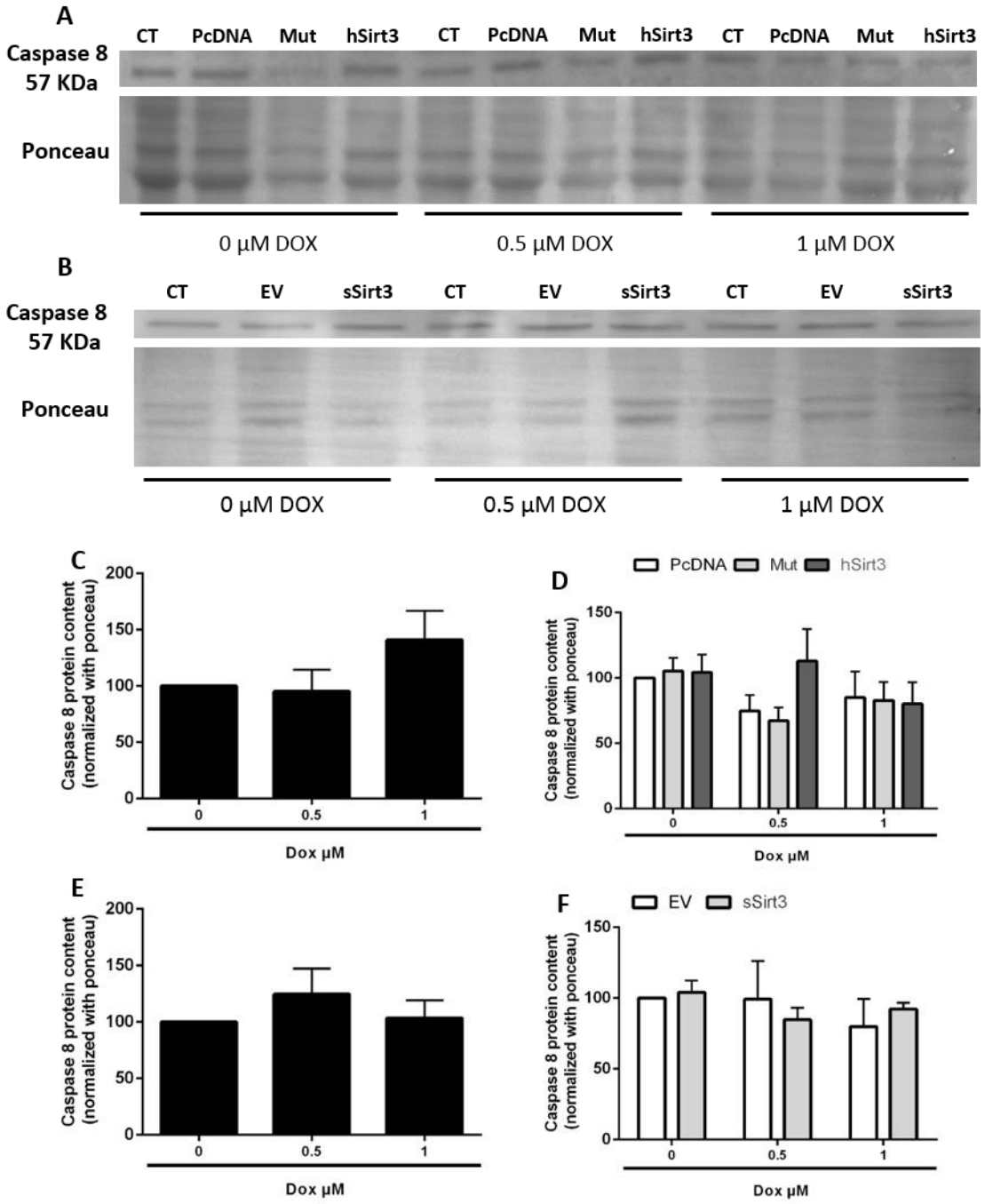

Figure 9– Caspase 8 protein content did not change with DOX treatment nor Sirt3 over/underexpressiom: Caspase 8 protein content was analyzed using a commercial antibody by western blotting, after transfection followed by DOX treatment. Representative western blot of Caspase 8 (≈ 57 KDa) protein expression and graphical representation of overexpression experiment (A, C and D) and underexpression (B, E and F). Data represents Mean ± SEM of 3 or 4 independent experiments. Statistical analysis was performed by using one-way ANOVA for C and E, and two-way ANOVA for D and F. $p < 0.05$ is considered statistically significant.

Caspase 9, a component of the intrinsic pathway, was also analyzed by western blotting. With the commercial antibody was detected 3 different bands of caspase 9: pro-caspase 9 (≈ 45 kDa), cleaved large fragment (≈ 35/37 kDa) and the fully cleaved caspase 9 (≈ 25 kDa) (Fig. 10A). The overexpression experiment was performed using H9c2 cardiomyoblasts, which underwent transfection and were next treated with DOX. H9c2 control cells showed a significant increase in caspase 9 related bands after 1 μM DOX treatment. Relatively to cleaved caspase 9, the increase was also visible for 0.5 μM DOX (Fig. 10B, 10D and 10F)). Control PcDNA transfected cells exhibited an increase of all caspase 9 fragments with DOX, however this alteration was not statistically significant. The exception occurred for caspase 9 and 0.5 μM DOX. Besides the increased large fragment for mutant and cleaved fragment for hSirt3, both in 1 μM DOX, hSirt3 and mutant hSirt3 overexpression cells showed no changes in caspase 9 protein content (Fig. 10C, 10E and 10G).

Caspase 9 was also assessed after Sirt3 underexpression, using the same antibody described above. Although control cells showed an increase of caspase 9 with both DOX concentrations, this increase was not statistically significant (Fig. 11B, 11D and 11F). On the other hand, pro-caspase 9 was decreased in sSirt3 cells with 0.5 and 1 μM DOX compared to sSirt3 cells without DOX (Fig. 11C). In the condition without DOX, sSirt3 cells contained more cleaved caspase 9 when compared to control PcDNA transfected cells (Fig. 11G). However, this did not happen with DOX treatment.

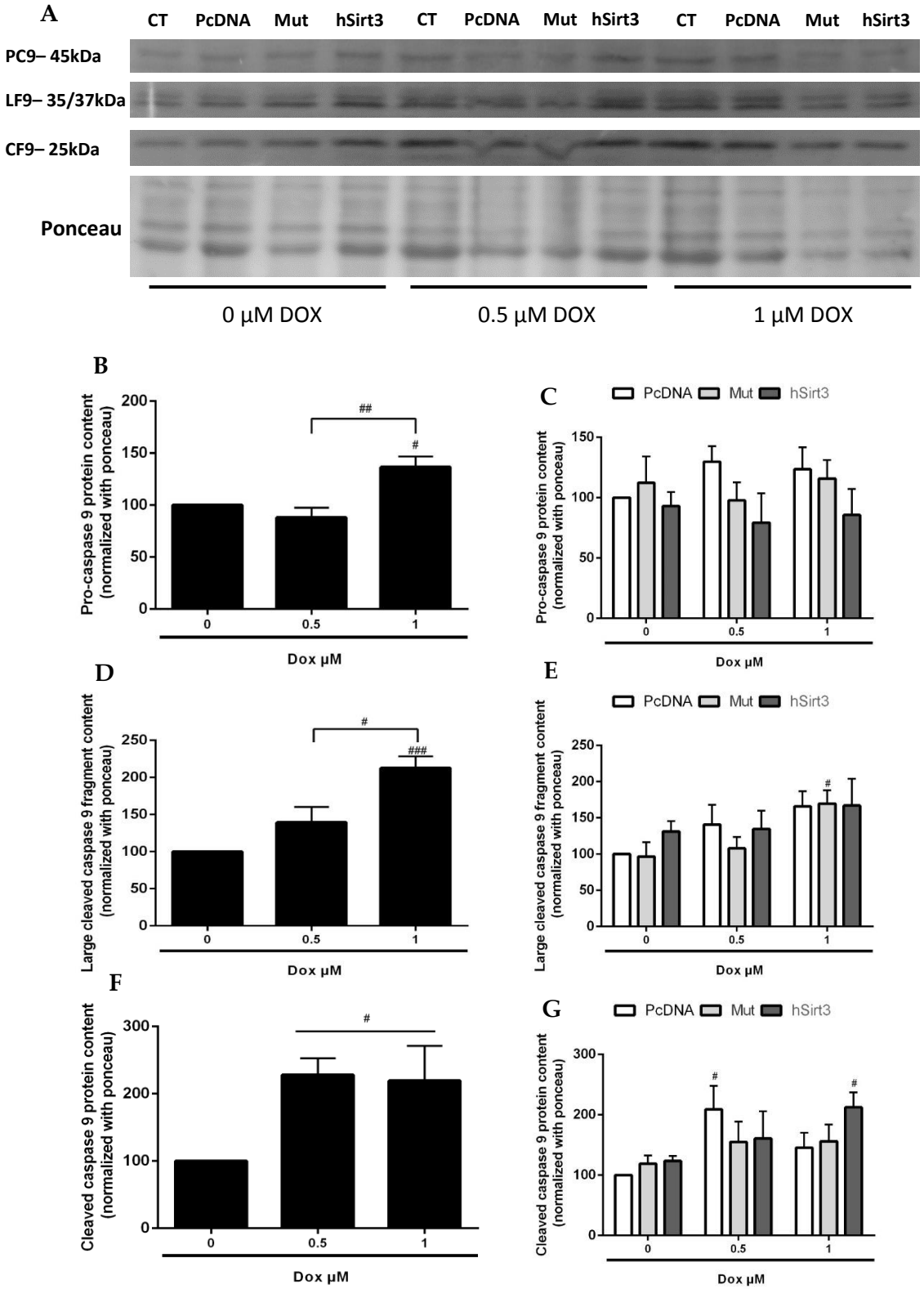

Figure 10– Effect of DOX and Sirt3 overexpression in Caspase 9 protein content: The experiment was performed after transfection and DOX treatment. A) Representative western blot of caspase 9: pro-caspase 9 (PC9) (≈ 45 kDa), large cleaved caspase 9 fragment (LF9) (≈ 35/37 kDa) and fully cleaved caspase 9 (CF) (≈ 25 kDa). B, D and F) Control cardiomyoblasts with transfection reagent. Results are normalized to the control without DOX. C, E and G)

Overexpression experiment using empty vector cells as control (PcDNA), Sirt3 deacetylase mutant cells (Mut) and Sirt3 overexpression cells (hSirt3). Results are normalized to the control, no DOX, transfected cells. Data represents Mean ± SEM of 3 – 4 independent experiments. Statistical analysis was performed by using one-way ANOVA for B, D and F, and two-way ANOVA for C, E and G. One symbol= p< 0.05, two symbols= p< 0.01 and three symbols= p<0.001. # Analysis made inside the same transfection condition.

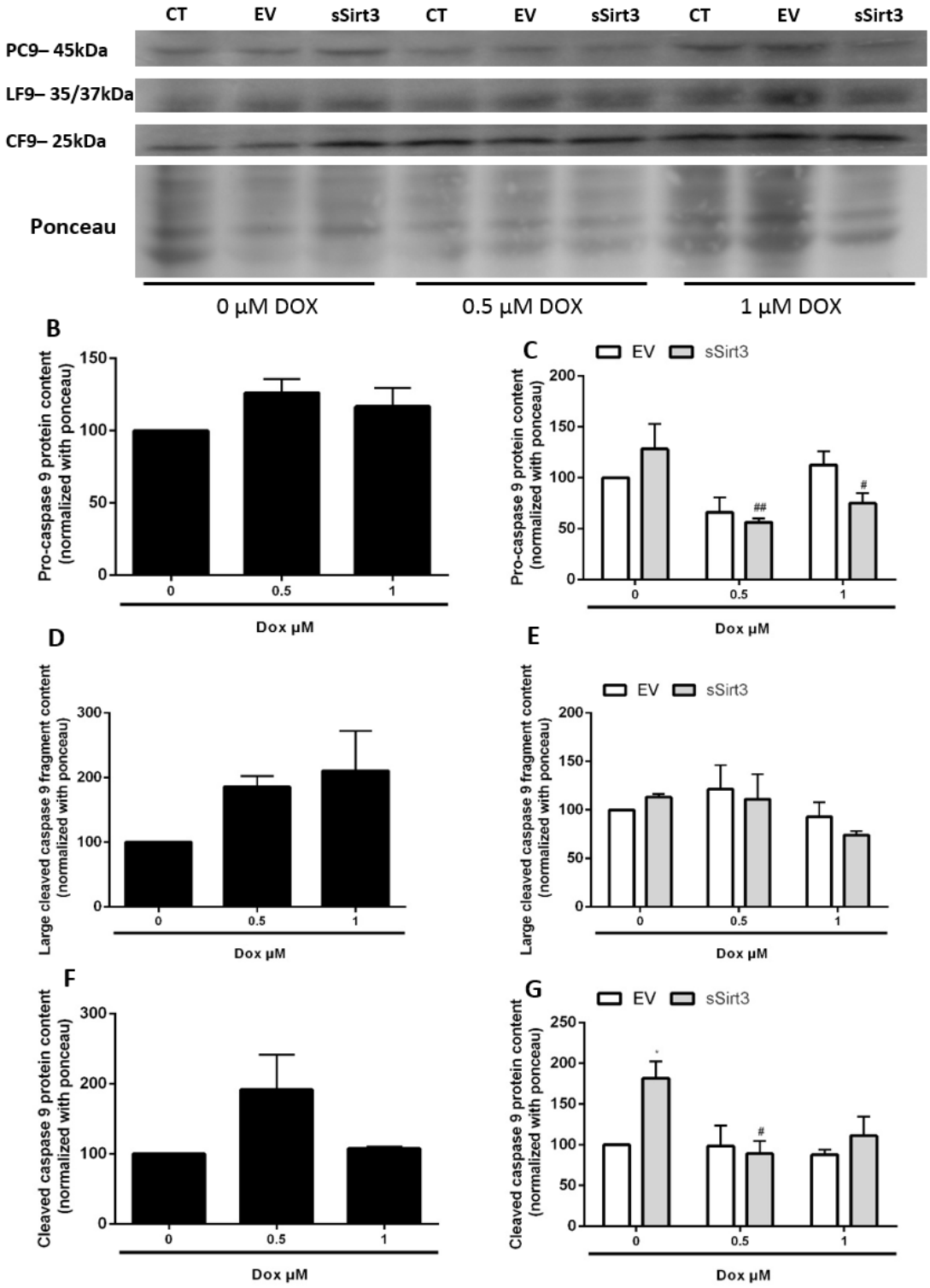

Figure 11– Effect of DOX and Sirt3 underexpression in Caspase 9: The experiment was performed after transfection and DOX treatment. A) Representative western blot of caspase 9:

pro-caspase 9 (PC9) (≈ 45 kDa), large cleaved caspase 9 fragment (LF9) (≈ 35/37 kDa) and fully cleaved caspase 9 (CF 9) (≈ 25 kDa). B, D and F) Control cardiomyoblasts with transfection reagent. Results are normalized to the control untreated cells. C, E and G) Underexpression experiment using empty vector cells as control (EV) and Sirt3 silenced cells (sSirt3). Results are normalized to the control, no DOX, transfected cells. Data represents Mean ± SEM of 3 – 4 independent experiments. Statistical analysis was performed by using one-way ANOVA for B, D and F, and two-way ANOVA for C, E and G. One symbol= $p< 0.05$ and two symbols= $p< 0.01$. # Analysis made inside the same transfection condition. * vs control of the same concentration of DOX.

The effector caspase 3 is activated by caspases involved in the extrinsic and intrinsic apoptotic pathway, interacting with the caspases mentioned above. Using a commercial antibody pro-caspase 3 (≈ 35 kDa) and cleaved caspase 3 (≈ 17 kDa) were also analyzed by western blotting. In overexpression assays, pro-caspase and cleaved caspase 3 increased in a concentration-dependent manner in control cells. However, the increase in cleaved caspase 3 was larger. H9c2 control cells showed a 4-fold and 7-fold increased cleaved caspase with 0.5 and 1 μM of DOX, respectively (Fig.12B and 12D). Pro-caspase 3 appeared not to change after Sirt3 overexpression (Fig. 12C). Once again, cleaved caspase 3 showed a large increase in all conditions of overexpression assay with DOX treatment. Curiously, hSirt3 cells showed a significant increase of cleaved caspase 3 when compared to control PcDNA transfected cells and hSirt3 mutant cells (Fig. 12E). During underexpression, H9c2 control cells also showed an increase of both caspases with DOX treatment, being again the increase of cleaved caspase 3 higher. For control EV cells and sSirt3 cells, pro-caspase 3 did not change, but cleaved caspase 3 was also augmented with DOX (Fig. 13).

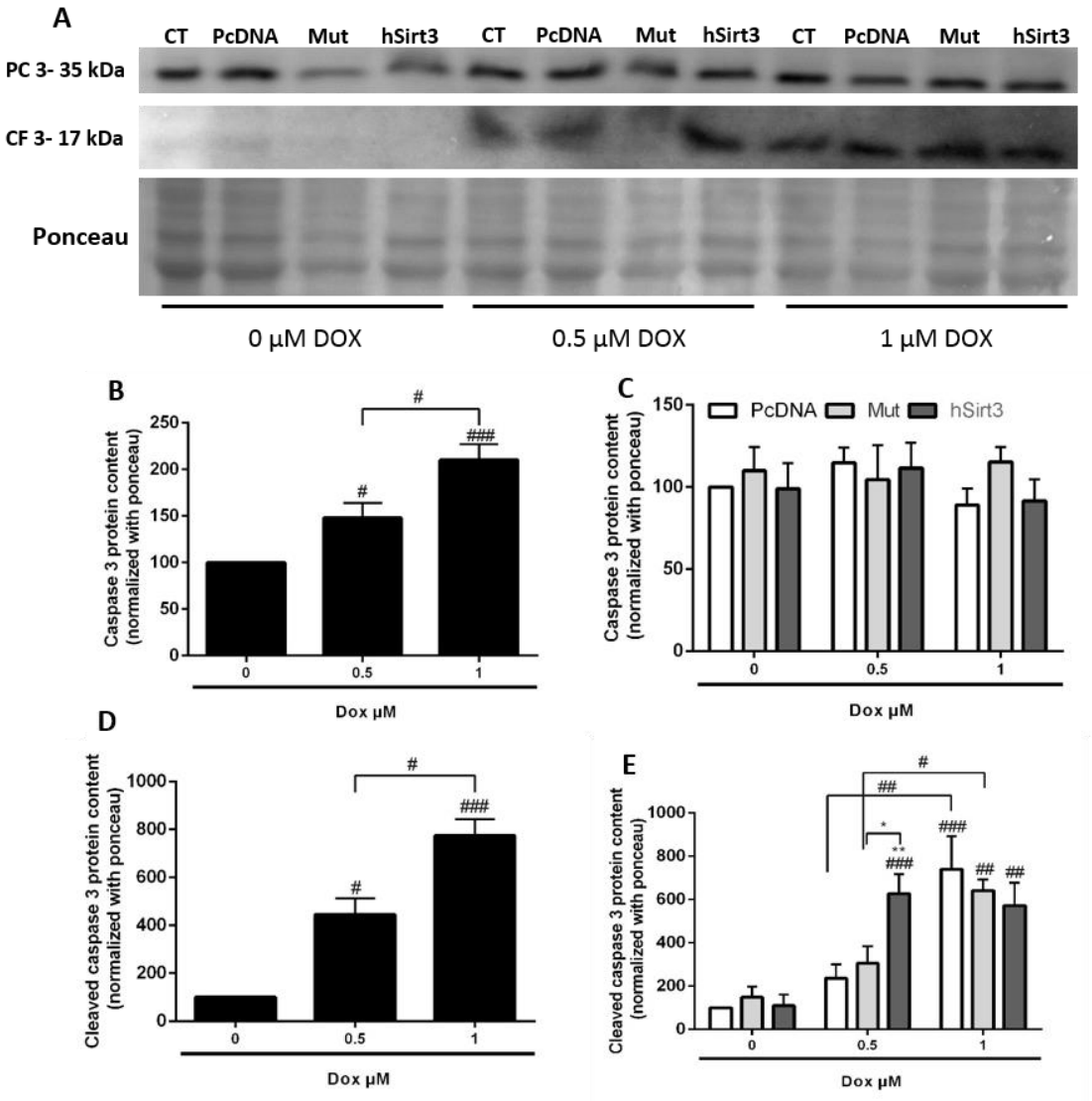

Figure 12– Effect of DOX and Sirt3 overexpression on Caspase 3 protein content: The experiment was performed after transfection and DOX treatment. A) Representative western blot of caspase 3: pro-caspase 3 (PC 3) (≈ 35 kDa) and cleaved caspase 3 (CF 3) (≈ 17 kDa). B and D) Control cells with transfection reagent. Results are normalized to the control without DOX. C and) Overexpression experiment using empty vector cells as control (PcDNA), Sirt3 deacetylase mutant cells (Mut) and Sirt3 overexpression cells (hSirt3). Results are normalized to the control, no DOX, transfected cells. Data represents Mean ± SEM of 3 – 4 independent experiments. Statistical analysis was performed by using one-way ANOVA for B and D, and two-way ANOVA for C and E. One symbol= $p< 0.05$, two symbols= $p< 0.01$ and three symbols= $p<0.001$. # Analysis made inside the same transfection condition. * vs control of the same concentration of DOX.

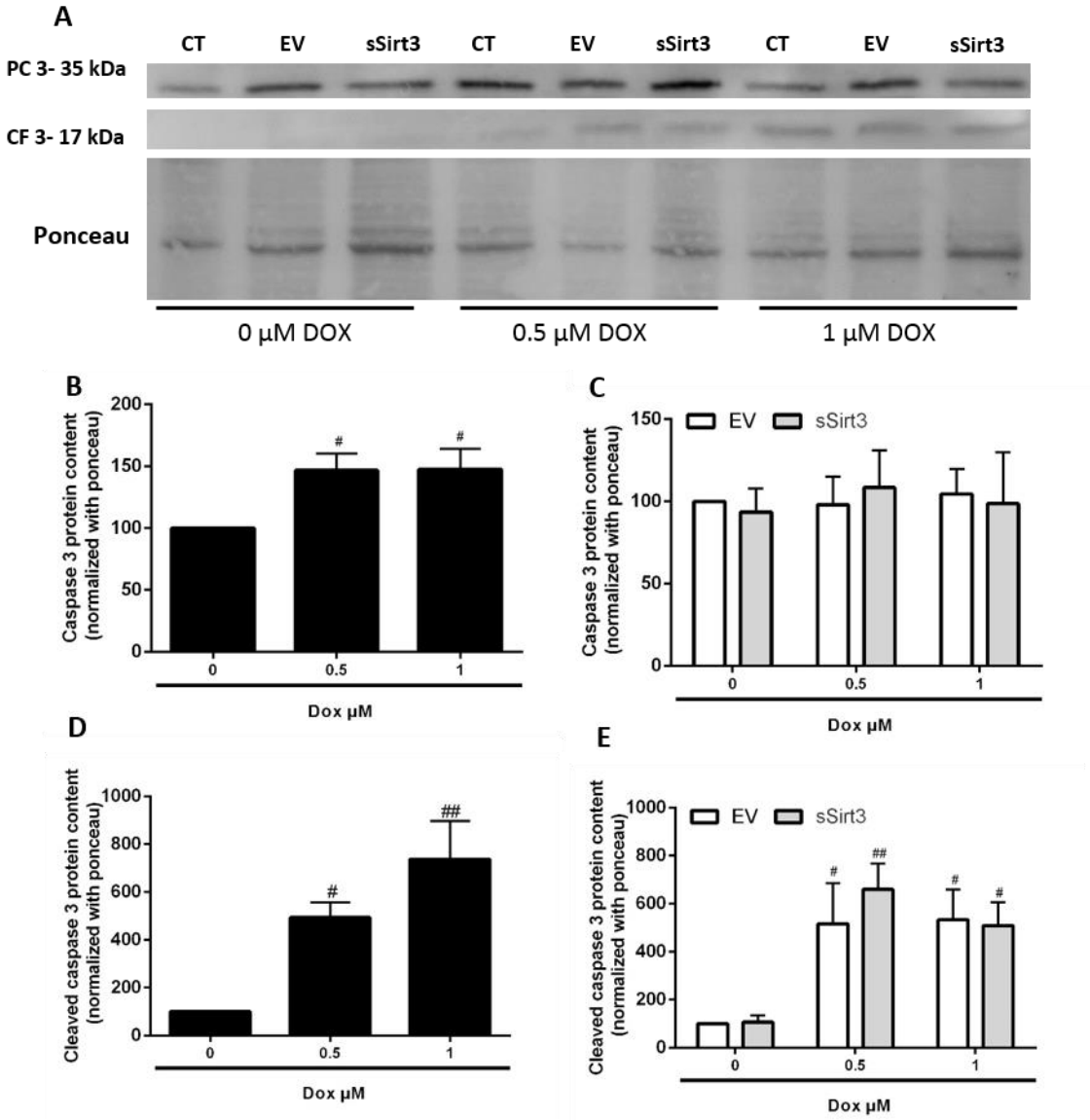

Figure 13– Effect of DOX and Sirt3 underexpression in Caspase 3 protein content: The experiment was performed after transfection and DOX treatment. A) Representative western blot of caspase 3: pro-caspase 3 (PC3) (≈ 35 kDa) and cleaved caspase 3 (CF 3) (≈ 17 kDa). B and D) Control H9c2 cells with transfection reagent. Results are normalized to the control without DOX. C and E) Underexpression assay using empty vector cells as control (EV) and Sirt3 silenced cells (sSirt3). Results are normalized to the control, no DOX, transfected cells. Data represents Mean ± SEM of 3 – 4 independent experiments. Statistical analysis was performed by using one-way ANOVA for B and D, and two-way ANOVA for C and E. One symbol= $p< 0.05$ and two symbols= $p< 0.01$ and. # Analysis made inside the same transfection condition.

3.1 Sirt3 decreases p53 over activation by DOX treatment

In order to analyze p53 and acetyl-p53 protein content, western blotting was again performed. H9c2 control cells showed a significant increase of p53 with both DOX

concentrations, which is concentration-dependent (Fig. 14C and 14E). Control PcDNA cardiomyoblasts also showed a significant increase of p53 in 0.5 and 1 μM treated cells. In 0.5 μM conditions, a significant decrease of p53 protein content was observed when comparing control PcDNA and hSirt3 overexpressing cells. hSirt3 mutant cells also presented a decrease in p53 content, however it was not statistically significant. After 1 μM DOX treatment, hSirt3 cells also showed a decreasing trend which was not significant (Fig. 14D). On the other hand, during Sirt3 underexpression assay, control EV transfected cells demonstrated again an increase of p53 with DOX treatment. Nevertheless, sSirt3 cells showed an increasing trend of p53 relatively to EV control cells (Fig. 14F).

4. Sirt3 overexpression decreases mitochondrial superoxide anion, but does not modulate SOD II protein content

To examine the effect of Sirt3 on superoxide anion production after DOX treatment, H9c2 cells transfected and DOX treated were dual-labeled with MitoSox Red and MitoTracker green. Because MitoSox selectively target mitochondria and is only oxidized by superoxide anion, it does not yield information about other ROS or RNS generating systems. MitoTracker Green is used to localize mitochondria, regardless of the mitochondrial membrane potential. The images obtained by fluorescence microscopy showed an increase of superoxide anion in control cells after DOX treatment (Fig. 15A, 15B and 15C). Mitosox Red fluorescence was also more intense in control PcDNA transfected cell when compared to control cells (Fig. 15D, 15E and 15F). The overexpression of Sirt3 appears to decrease the amount of superoxide anion in mitochondria in DOX conditions, being this decrease more visible with 0.5 DOX treatment (Fig. 15J, 15L and 15M).

SOD II protein content was also analyzed during Sirt3 overexpression and underexpression assay by western blotting. DOX treatment increased SOD II in control H9c2 cardiomyoblasts (Fig. 16C and 16E). In both assays, control transfected cells also showed an increase in the amount of SOD II, although just on EV cells treated with 1

μM of DOX was significant. However, Sirt3 transfection did not result in any alteration (Fig. 16D and 16F).

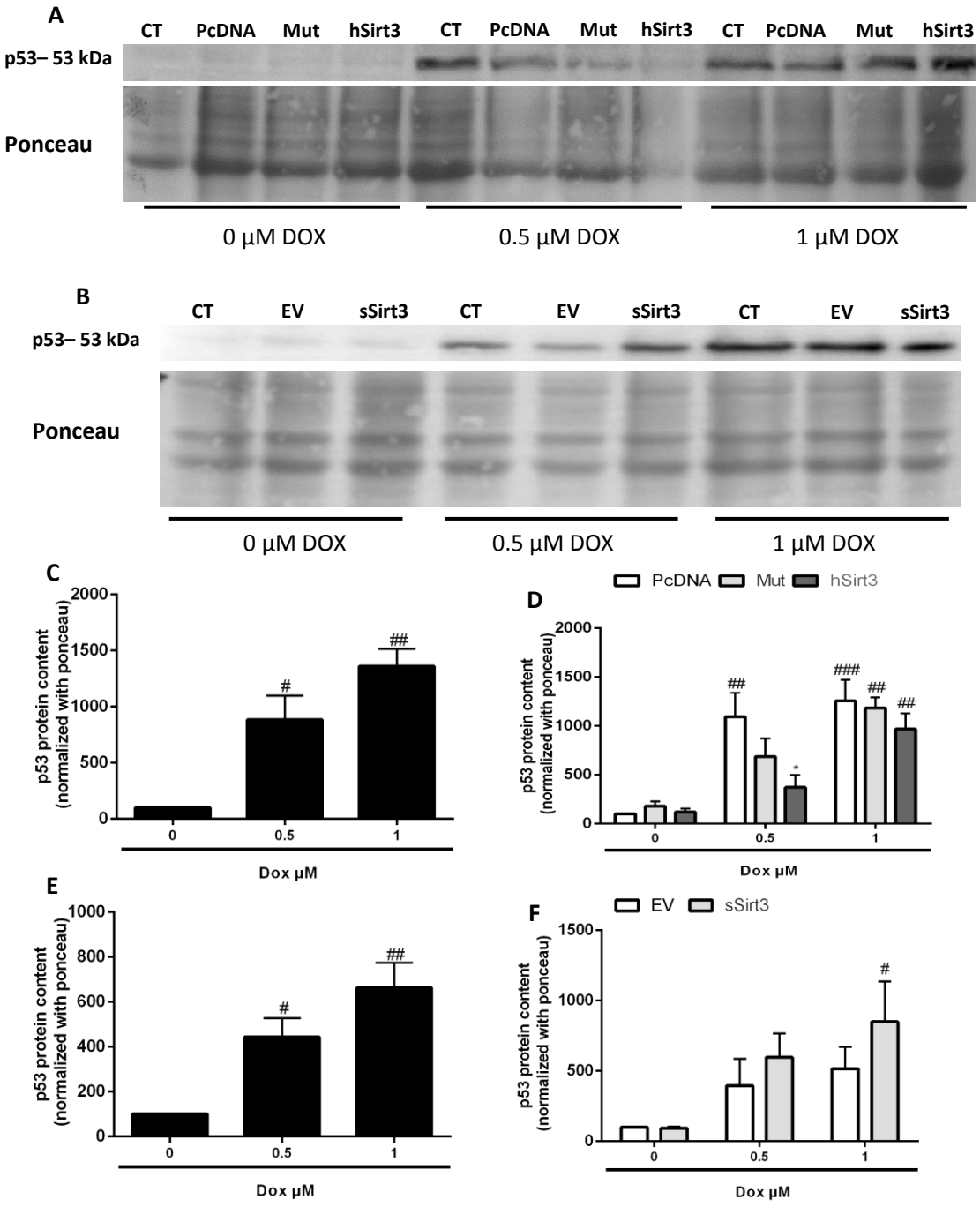

Figure 14– Sirt3 overexpression decreases p53 after DOX treatment: p53 protein content was analyzed using a commercial antibody by western blotting, after transfection and DOX treatment. Representative western blot of p53 (≈ 53 KDa) protein expression in overexpression (A) and underexpression (B). C and E) Graphical representation of overexpression and underexpression control cells with DOX, respectively. Results are normalized to the control without DOX. D) Overexpression experiment using empty vector cells as control (PcDNA), Sirt3 deacetylase mutant cells (Mut) and Sirt3 overexpression cells (hSirt3). F) Underexpression assay

using empty vector cells as control (EV) and Sirt3 silenced cells (sSirt3). Results are normalized to the control, no DOX, transfected cells. Data represents Mean ± SEM of 3 or 4 independent experiments. Statistical analysis was performed by using one-way ANOVA for C and E, and two-way ANOVA for D and F. One symbol= $p< 0.05$, two symbols= $p< 0.01$ and three symbols= $p<0.001$. # Analysis made inside the same transfection condition. * vs control of in the same concentration of DOX.

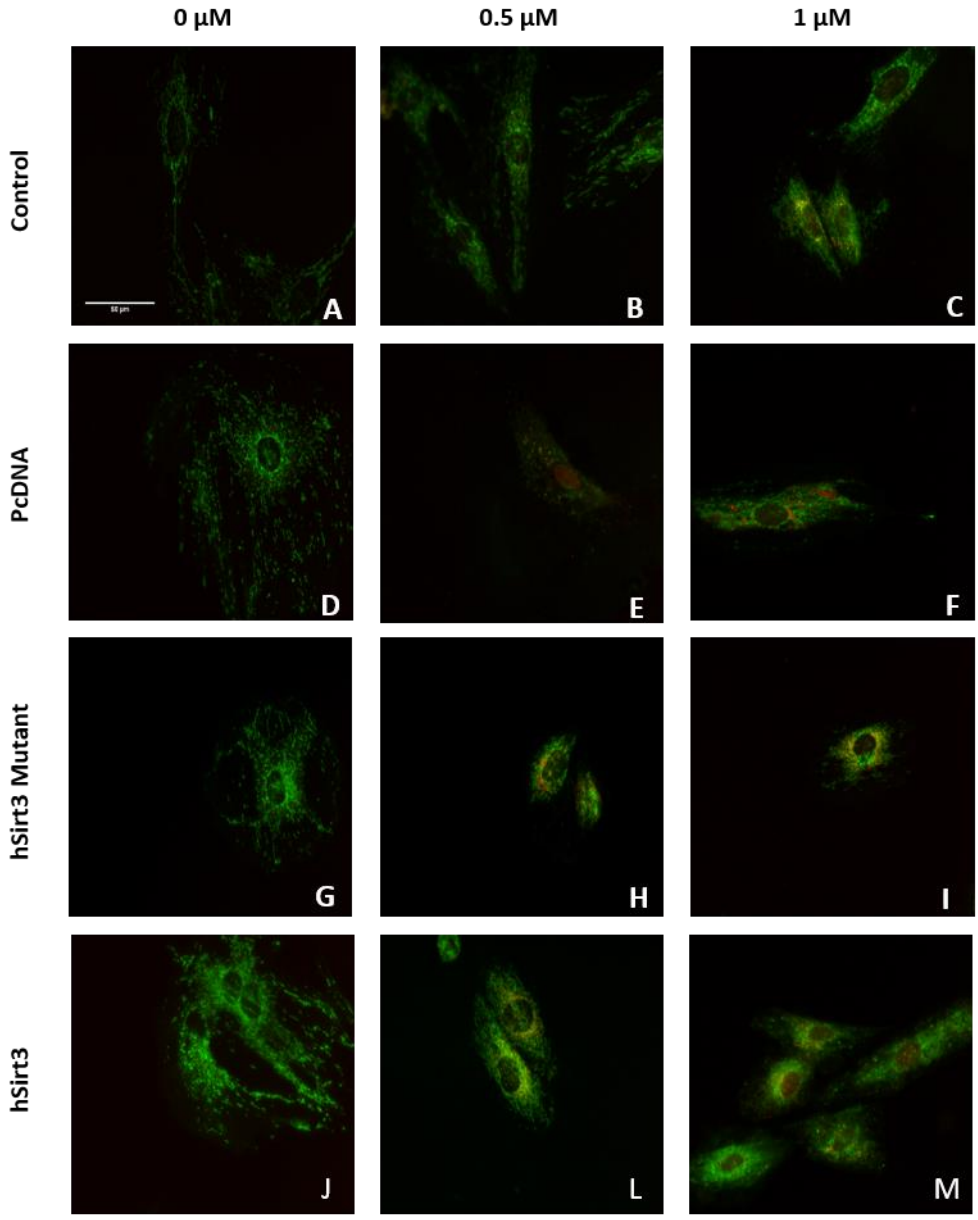

Figure 15– Sirt3 overexpression decreases mitochondrial superoxide anion in H9c2 Cardiomyoblasts: Mitochondrial superoxide anion was evaluated using MitoSOX red probe and mitochondria was counterstained with MitoTracker green, which stains the mitochondrial network. Images were acquired by fluorescence microscopy using a 40x objective. A) Control cells without DOX. B and C) Control cells treated with 0.5 and 1 µM of DOX. D, E and F) Control PcDNA transfected cells with 0, 0.5 and 1 µM of DOX. G, H and I) Sirt3 mutant overexpression cells under the same DOX conditions. J, L and M) Sirt3 overexpression cells

without treatment and with 0.5 and 1 μM of DOX, respectively. Data represents 2 independent experiments.

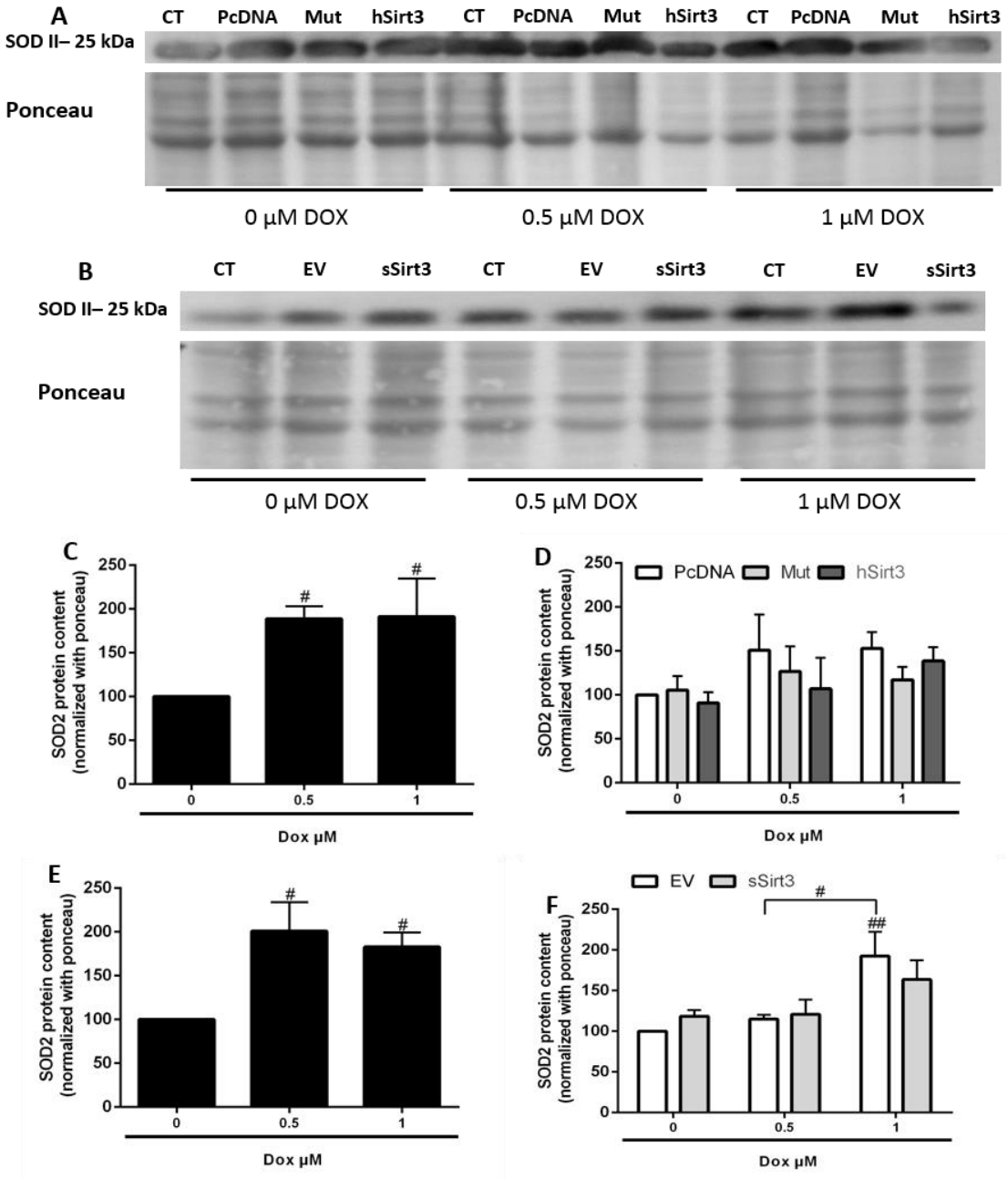

Figure 16– Sirt3 does not change SOD II protein content in H9c2 Cardiomyoblasts: SOD II protein content was analyzed using a commercial antibody, after transfection and DOX treatment. Representative western blot of SOD II (≈ 25 KDa) protein expression in overexpression (A) and underexpression (B). C and E) Graphical representation of overexpression and underexpression control cells with DOX, respectively Results are normalized to the control without DOX. D) Overexpression experiment using empty vector cells as control (PcDNA), Sirt3 deacetylase mutant cells (Mut) and Sirt3 overexpression cells (hSirt3). F) Underexpression assay using empty vector cells as control (EV) and Sirt3 silenced cells (sSirt3). Results are normalized to the control, no DOX, transfected cells. Data represents

Mean ± SEM of 3 or 4 independent experiments. Statistical analysis was performed by using one-way ANOVA for C and E, and two-way ANOVA for D and F. One symbol= $p< 0.05$ and two symbols= $p< 0.01$. # Analysis made inside the same transfection condition.

5. hSirt3 overexpression protects against DOX-induced mitochondrial fragmentation in H9c2 Cardiomyoblasts

By using fluorescence microscopy, alterations in mitochondrial morphology were evaluated using TMRM, which accumulates inside polarized mitochondria. H9c2 control cells without DOX had filamentous polarized mitochondria (Fig. 17A). Treatment with 0.5 and 1 μM DOX caused breakage of mitochondrial filaments (Fig. 17B and 17C). In control PcDNA transfected cells the same mitochondrial fragmentation was also visible. However, without DOX, these cells also showed similar effect, probably due to vector toxicity (Fig. 17D, 17E and 17F). When Sirt3 was overexpressed, cells acquired again the filamentous polarized mitochondria phenotype, in the presence or absence of DOX (Fig. 17J, 17L and 17M) This was not evident in Sirt3 mutant overexpression conditions (Fig. 17G, 17H and 17I).

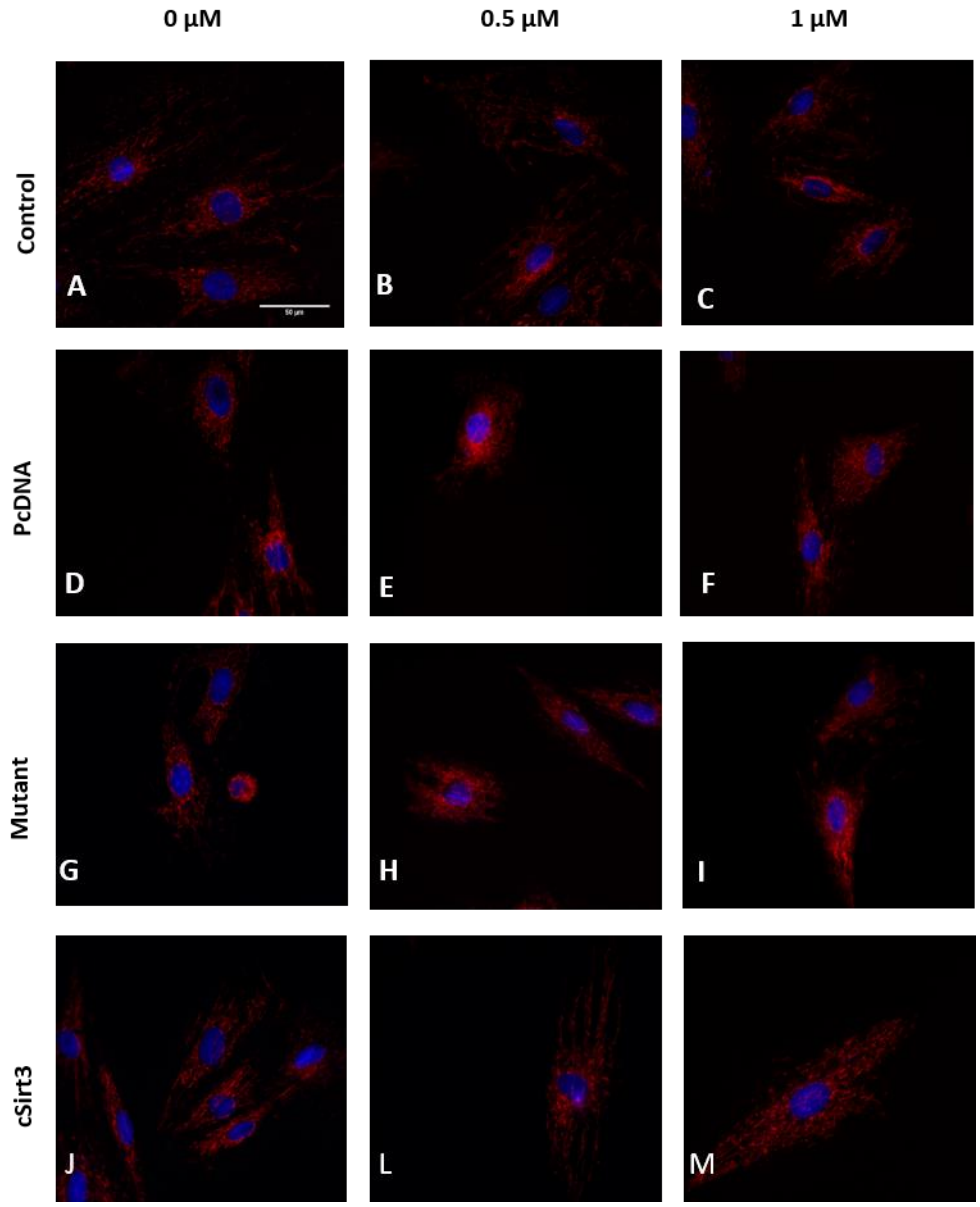

Figure 17– Sirt3 overexpression protects against DOX-induced mitochondrial fragmentation in H9c2 Cardiomyoblasts: Epifluorescence microscopy images showing double labeling with Hoechst 33343 (blue) and TMRM (red). Images were acquired by using a 40x objective. A) Control cells without DOX. B and C) Control cells treated with 0.5 and 1 µM of DOX. D, E and F) Control PcDNA transfected cells with 0, 0.5 and 1 µM of DOX. G, H and I) Sirt3 mutant overexpression cells with the same DOX conditions. J, L and M) Sirt3 overexpression cells without treatment and with 0.5 and 1 µM of DOX, respectively. Data represents 2 independent experiments.

6. Protein content of mitochondrial complexes undergoes alterations following DOX treatment and Sirt3 transfection

The protein content of OXPHOS complex was assessed by western blotting, by using a cocktail of commercial antibodies. This cocktail contains 5 monoclonal antibodies against one subunit of each mitochondrial complex: NDUFB8 subunit of complex I (20 kDa), SDHB of complex II (30 kDa), UQCRC2 subunit of complex III (47 kDa), MTCO1 of complex IV (39 kDa) and ATP5A of ATP synthase (53 kDa). During overexpression assay, control H9c2 cells that only contained transfection reagent showed alterations of complexes protein content after DOX treatment. The protein amount of all subunits increased significantly with DOX treatment, except complex IV subunit which although also increased, the difference was not significantly. The greatest increase occurred on complex I and II, with 1 μM DOX. Complex I showed a 3.5-fold increase in protein content while complex II showed a 2.5-fold increase (Fig. 18B, 18D, 18F, 18H and 19J). In hSirt3 overexpression cells with 0.5 μM DOX, complex I subunit was significantly increased comparing to the same condition without DOX, but also showed an increasing trend when compared to control PcDNA transfected cells (Fig. 18C). A similar trend was visible on SDHB and ATP5A subunit (Fig. 18E and 18K). Complex III subunit was increased in Sirt3 overexpression cells after treatment with 0.5 μM of DOX (Fig. 18G). Regarding complex IV subunit, Sirt3 overexpression with 0.5 μM DOX resulted in increase of the subunit. However, with 1 μM DOX, hSirt3 and hSirt3 mutant overexpression produced a decrease in MTOC1 protein content (Fig 18I). On the other hand, in underexpression experiments, control cells just showed an increase of complex I and II after DOX treatment (Fig. 19B and 19D). Sirt3 silencing did not promote significant alterations in protein content of complex I and V. Nevertheless, complex I appeared to be decreased in 1 μM DOX condition after silencing of Sirt3 (Fig. 19C and 19I). Interestingly complex II increased after Sirt3 silencing in cells without DOX, but in the presence of DOX no alterations were visible (Fig. 19E). Regarding complex III subunit, silencing induced a reduction around 50% of UQCRC2 subunit, with 0.5 μM DOX (Fig. 19G).

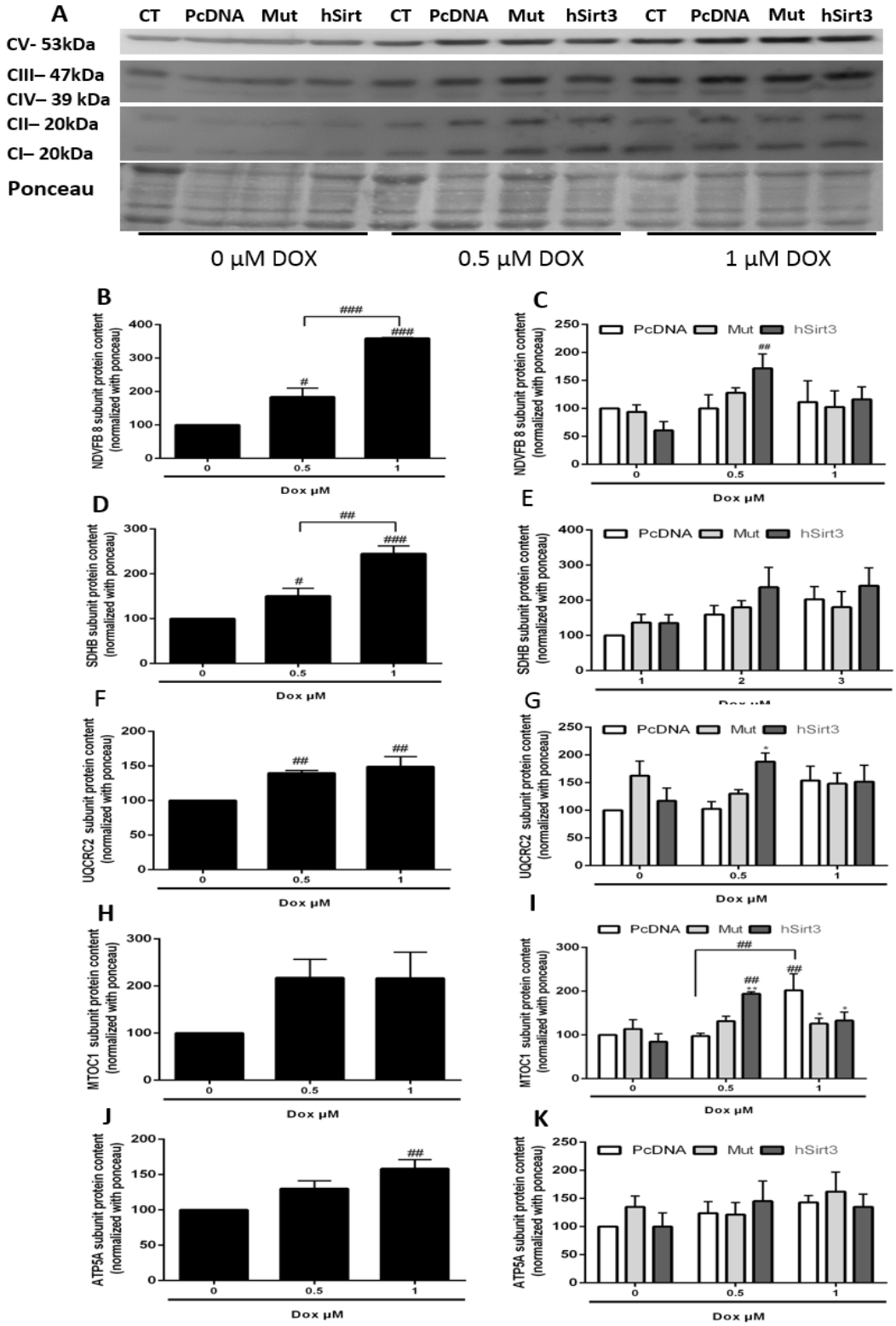

Figure 18– Sirt3 overexpression and OXPHOS complexes in H9c2 Cardiomyoblasts: A) OXPHOS complexes protein content was analyze by WB: NDUFB8- CI (20 kDa), SDHB- CII (30 kDa), UQCRC2- CIII (47 kDa), MTCO1- CIV (39 kDa) and ATP5A- CV(53 kDa). B, D F, H and J) Control cells with transfection reagent. Results are normalized to the control without DOX. C, E,

G, I and K) Overexpression experiment using empty vector cells as control (PcDNA), Sirt3 mutant cells (Mut) and Sirt3 overexpression cells (hSirt3). Results are normalized to the control, no DOX, transfected cells. Data represents Mean ± SEM of 3 or 4 independent experiments. Statistical analysis was performed by using one-way ANOVA or two-way ANOVA. One symbol= p< 0.05, two symbols= p< 0.01 and three symbols= p<0.001. # Analysis made inside the same transfection condition. * vs control of the same concentration of DOX.

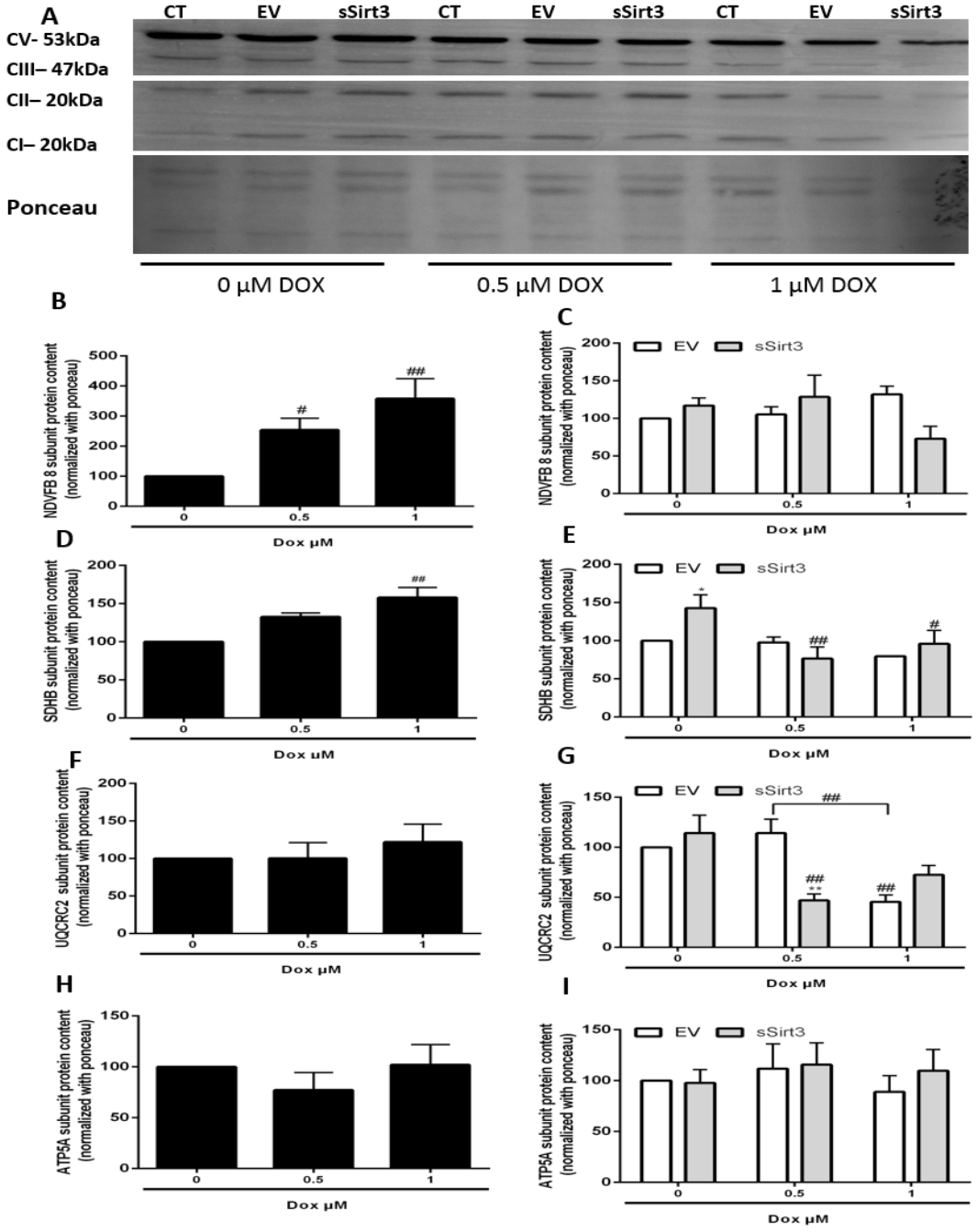

Figure 19– Sirt3 underexpression and OXPHOS complexes in H9c2 Cardiomyoblasts: A) Representative blot of OXPHOS complexes: NDUFB8- CI (20 kDa), SDHB- CII (30 kDa), UQCRC2- CIII (47 kDa), MTCO1- CIV (39 kDa) and ATP5A- CV(53 kDa). B, D F and H) Control H9c2 cells with transfection reagent. Results are normalized to the control without DOX. C, E, G and I) Underexpression assay using empty vector cells as control (EV) and Sirt3 silenced cells (sSirt3). Results are normalized to the control, no DOX, transfected cells. Data represents Mean

± SEM of 3 or 4 independent experiments. Statistical analysis was performed by using one-way ANOVA or two-way ANOVA. One symbol= p< 0.05, two symbols= p< 0.01 and three symbols= p<0.001. # Analysis made inside the same transfection condition. * vs control of the same concentration of DOX.

7. Sirtuins mRNA levels after Sirt3 transfection and DOX treatment in H9c2 cells

Using RT-PCR, mRNA levels of Sirt1 and two other mitochondrial sirtuins, Sirt4 and Sirt5, were assessed. However, due to the small amount of Sirt4 in H9c2 cells this transcript was not analyzed. In control cells, Sirt1 appeared to increase with 0.5 μM DOX but to decrease with 1 μM (Fig. 20A). Control PcDNA transfected cells also showed the same pattern (Fig. 20B). By in turn, Sirt5 decreased significantly with both DOX concentrations in control cells and control transfected cells (Fig. 20C). On the other hand, Sirt3 overexpression did not result in alterations of Sirt1 and Sirt5 transcripts (Fig. 20B and 20D).

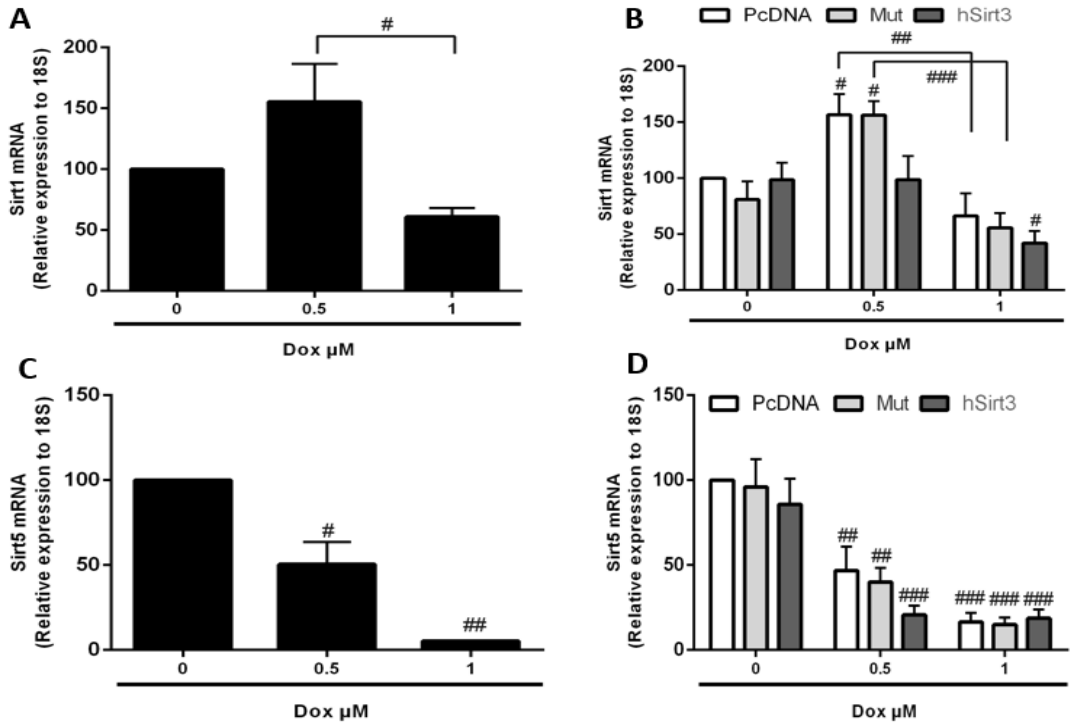

Figure 20- Sirt1 and Sirt5 mRNA levels after Sirt3 overexpression and DOX treatment in H9c2 Cardiomyoblasts: Sirt1 and Sirt5 mRNA levels were quantified by RT-PCR in control cells with and without DOX (A and C) and in control PcDNA, hSirt3 mutant and hSirt3 overexpressing cells with 3 DOX concentrations (B and D). Results are normalized to the control, no DOX, transfected cells. Data represents Mean ± SEM of 2-3 independent

experiments. Statistical analysis was performed by using one-way ANOVA and two-way ANOVA. One symbol= $p< 0.05$, two symbols= $p< 0.01$ and three symbols= $p<0.001$. # Analysis made inside the same transfection condition.

Chapter 4 – Discussion/Conclusion

Discussion

Doxorubicin is one of most potent anticancer agent and has been used against wide range of tumors. However the dose-dependent cardiotoxicity induced by DOX compromises the clinical application [29]. DOX-induced cardiotoxicity has a strong mitochondrial component and a range of different mechanism are behind it, such as cell death and disruption of mitochondrial homeostasis. Nevertheless, oxidative stress has been implicated as a major mechanism on cardiac cells [12, 25]. Sirtuin 3, the major mitochondrial deacetylase, is described as protecting mitochondria against oxidative stress, contributing to cell survival [89, 90].

The objective of the present study was understand the role of Sirt3 on cardiomyoblasts treated with DOX, based on our hypothesis that Sirt3 protects H9c2 cells against DOX-induced cardiotoxicity. To perform the study, we used concentrations present in plasma of patients treated with DOX (0.5 and 1 μM) [26].

H9c2 cells showed a low endogenous protein expression and mRNA levels of Sirt3, unless overexpressed with a human Sirt3-flag or a catalytically inactive HY mutant form of hSirt3, in which a single amino acid residue has been modified (histidine-to-tyrosine at amino acid residue 248). In fact, some authors have already described a low endogenous amount of Sirt3 in cardiomyocytes or H9c2 cell line [112, 113]. Curiously, control cells with transfection reagent in underexpression experiments showed an increase of Sirt3 short-form with DOX. It was previously observed in soleus muscle that an acute DOX treatment did not affect the expression of Sirt1 and Sirt3 nor lysine acetylation status [114]. However, when Sundaresan et al. (2008) exposed cardiomyocytes to stress stimuli, the treatment elevated the levels of Sirt3 long-form, but Sirt3 short-form did not change [89]. On the other hand, DOX treatment in H9c2 cells induced an increase of Sirt2 protein content [115]. Probably due to low amount of endogenous Sirt3 in H9c2 cells, the decrease of Sirt3 protein content by silencing was not detected in cells without treatment and with 0.5 μM of DOX, although in 1 μM DOX increased the amount of Sirt3 in H9c2 cells.

Although the mechanism of DOX-induced cell death is not totally understood, it is clear that DOX promote cell death in cardiomyocytes [30, 37, 115]. Our results also showed a decrease of cell mass and live cells for both DOX concentrations (0.5 and 1 μM), and an increase in dead cells. DOX treatment in control cells also increased caspase 3 and 9 protein content, but caspase 8 did not show any alteration. These results are supported by previous studies [114, 116]. Agreeing with Sardão et al. (2009) [34], p53 protein content increased with DOX, in a concentration-dependent manner. Regarding live/dead assay, it is curious the decrease of dead cells in transfected cells with DOX. Probably it is due to vector toxicity that can influence the result, but further experiments are needed to explain this. On the other hand, hsirt3 cells showed a trend increasing of live cells comparing to control PcDNA transfected cells. Although Sirt3 did not change caspase protein content, caspase activity can be altered, although this was not measured in the present work. p53 decreased after overexpression and increased after Sirt3 underexpression, when compared to control transfected cells. From the results one can conclude that p53 activation is an important pathway in DOX-induced cell death. However, as mentioned before (in section 2.3.2) cell death-induced by DOX can be dependent or independent of p53 [34, 62]. Besides mediating cell fate through nuclear and transcription components, p53 can also induce alteration of mitochondrial membrane potential, leading to cyt c release and consequently apoptosis [117, 118]. H9c2 cardiomyoblasts treated with DOX showed a translocation of Bax and p53 to mitochondria [34], where Sirt3 interacts and deacetilates p53, abrogating its activity [118]. p53 inhibition leads to a decrease of pro-apoptotic protein Bax [34], which can be also decrease by Sirt3 through ku70 protein interaction, under stress conditions [89]. Thus, under stress conditions, increased expression of Sirt3 probably protects cardiomyocytes by interacting with p53 and preventing the translocation of Bax to mitochondria and blocking cyt c release.

Several reports consider that DOX-induced cell death is associated with increased oxidative stress. Our work also showed an increase of superoxide anion production with both DOX concentrations. One of the causes attributed to the increased ROS in cardiomyocytes after DOX treatment is the decrease in SOD II [115, 119, 120]. However, we found an increase of SOD II protein content in control H9c2 cells with DOX, which

was also detected by Tokudome et al using cardiac myocytes [121]. Sirt3 appeared to decrease the amount of superoxide anion, especially with 0.5 μM DOX. Since Sirt3 deacetylates and activates SOD II [101], its protective effect against ROS can be due to SOD II activation and not so much by increasing its amounts. Calenic et al. (2013) suggested that in response to oxidative stress, similar to Sirt6, Sirt3 induces protective mechanism against genotoxicity [117].Agreeing with this, another recent study found a new Sirt3 target, the human 8-oxoguanine-DNA glycosylase 1 (OGC1). Its deacetylation by Sirt3 prevented the degradation and controlled the activity of OGC1, playing a critical role in repairing mtDNA damage and preventing apoptosis under oxidative stress [122].

Using TMRM, a fluorescence probe dependent of mitochondrial potential, mitochondrial morphology was assessed. In our work, mitochondrial depolarization and mitochondrial network fragmentation induced by low DOX concentrations was identified. This effect was more evident in control PcDNA transfected cells, probably due to subjacent vector toxicity. Consistent with our work, other works also showed a decrease in mitochondrial potential after DOX treatment [115, 120]. Sardão et al demonstrated the decrease of membrane potential in H9c2 cells with low DOX concentrations. In fact, by using higher DOX concentrations, such as 20 and 50 μM, the mitochondrial network still accumulated TMRM [26]. When Sirt3 was overexpressed, this protein was able to prevent the mitochondrial fragmentation induced by DOX, however the same did not happen with Sirt3 mutant overexpression. The protective effect conferred by Sirt3 was perhaps due to its deacetylase activity. Recently, it was demonstrated that Sirt3 binds and activate, via deacetylation, the fusion protein OPA1. During stress conditions, including DOX treatment in cardiomyocytes, Sirt3 preserved the normal tubular shape of mitochondria. In HeLA cells overexpressing WT and mutant Sirt3, just Sirt3 WT preserved mitochondrial morphology, being consistent with our work [113].

During our experiments, the protein content of different subunits of OXPHOS complexes was assessed by western blot. After DOX treatment, in underexpression and overexpression control cells, an increase of NADH dehydrogenase and succinate

dehydrogenase subunits content was observed. Regarding the other complexes, control overexpression cells showed an increase that did not happen in underexpression control cells. Since the transfection reagent was different depending on the experiment, it can be the cause of the difference in OXPHOS protein content. The literature usually shows measurements of OXPHOS complex activity. We instead measured protein content, with differences possibly existing between both. Concerning protein content alterations, another study with heart mouse homogenates and H9c2 cells did not show any variation, however the DOX concentration used here was lower [46]. Contrarily, another study demonstrated an increase of complex II protein content in heart lysates [123]. Moreover, Complex I and II activity is often reported decreased after DOX treatment [46, 124]. Thus, the increase of protein content of those complexes can be due to a compensatory mechanism in order to revert the loss of activity observed after DOX treatment. During overexpression, Sirt3 appeared to increase the amount of all complexes with 0.5 μM DOX but not with 1 μM DOX. On the other hand, complex III was decreased by Sirt3 underexpression and after 0.5 μM of DOX. These results can indicate that different concentrations of DOX can affect the role of Sirt3 within the cell. The influence of Sirt3 under stress conditions in mitochondrial OXPHOS components in terms of protein content is not well established, since the studies published so far related Sirt3 activity with preservation of complex activity.

Similarly to previously published data, Sirt3 overexpression and underexpression did not influence transcripts levels for other sirtuins, including Sirt1 and Sirt5 [125].

Taken together, the results of our study demonstrated that Sirt3 may confer protection against DOX-induced cardiotoxicity. However, there are still questions regarding the mechanisms involved and about the relationship between DOX concentration and protection afforded by Sirt3.

Conclusion

In conclusion, Sirt3 overexpression seems to result in increased protection against DOX-induced cardiotoxicity, possibly by decreasing p53 activation. The role of Sirt3 in inhibiting DOX toxicity, although still with a largely unknown mechanism, is worth developing, mainly the potential role of Sirt3-activating molecules.

Future Experiments

To further pursue this work and produce a manuscript for submission to a peer-reviewed scientific journal, the following experiments will be performed:

- SOD II activity, to understand if the protective effect of Sirt3 against ROS is due to the increase of SOD II activity.
- OXPHOS complexes activity, in order to find alterations under DOX treatment and the effect of Sirt3 under stress conditions.
- Measure ATP levels, to complement the previous task, this experiment will be performed to understand the efficiency of OXPHOS and the possible switch to glycolysis due to DOX treatment and reversal with Sirt3 overexpression.
- Evaluate the protein TOM20 content by Western blot, to determine a rough estimate on the amount of mitochondria.
- Analysis of mtDNA. The objective is to know if Sirt3 induces mitochondrial biogenesis.
- Assess Fusion/ fission proteins by western blot, to find which are influenced to Sirt3 and are involved in the protection against mitochondrial network fragmentation.
- Caspase activity assay, to understand if Sirt3 can change caspase activity even not interfering with caspase protein content.
- Measure Bcl-2 family protein content by western blot, to understand which proteins are modulated by Sirt3 overexpression.

Bibliography

1. Frezza, C. and E. Gottlieb, *Mitochondria in cancer: not just innocent bystanders.* Semin Cancer Biol, 2009. **19**(1): p. 4-11.
2. Modica-Napolitano, J.S., M. Kulawiec, and K.K. Singh, *Mitochondria and human cancer.* Curr Mol Med, 2007. **7**(1): p. 121-31.
3. Hoppins, S.C. and F.E. Nargang, *The Tim8-Tim13 complex of Neurospora crassa functions in the assembly of proteins into both mitochondrial membranes.* J Biol Chem, 2004. **279**(13): p. 12396-405.
4. Hom, J. and S.S. Sheu, *Morphological dynamics of mitochondria--a special emphasis on cardiac muscle cells.* J Mol Cell Cardiol, 2009. **46**(6): p. 811-20.
5. Wu, S., et al., *Mitochondrial oxidative stress causes mitochondrial fragmentation via differential modulation of mitochondrial fission-fusion proteins.* FEBS J, 2011. **278**(6): p. 941-54.
6. Chatterjee, A., E. Mambo, and D. Sidransky, *Mitochondrial DNA mutations in human cancer.* Oncogene, 2006. **25**(34): p. 4663-74.
7. Suski, J., et al., *Mitochondrial tolerance to drugs and toxic agents in ageing and disease.* Curr Drug Targets, 2011. **12**(6): p. 827-49.
8. Sardao, V.A., S.L. Pereira, and P.J. Oliveira, *Drug-induced mitochondrial dysfunction in cardiac and skeletal muscle injury.* Expert Opin Drug Saf, 2008. **7**(2): p. 129-46.
9. Gogvadze, V., S. Orrenius, and B. Zhivotovsky, *Mitochondria as targets for cancer chemotherapy.* Semin Cancer Biol, 2009. **19**(1): p. 57-66.
10. Gogvadze, V., S. Orrenius, and B. Zhivotovsky, *Mitochondria as targets for chemotherapy.* Apoptosis, 2009. **14**(4): p. 624-40.
11. Berridge, M.J., P. Lipp, and M.D. Bootman, *The versatility and universality of calcium signalling.* Nat Rev Mol Cell Biol, 2000. **1**(1): p. 11-21.
12. Pereira, G.C., et al., *Drug-induced cardiac mitochondrial toxicity and protection: from doxorubicin to carvedilol.* Curr Pharm Des, 2011. **17**(20): p. 2113-29.
13. Chen, Q., et al., *Production of reactive oxygen species by mitochondria: central role of complex III.* J Biol Chem, 2003. **278**(38): p. 36027-31.
14. Drose, S., *Differential effects of complex II on mitochondrial ROS production and their relation to cardioprotective pre- and postconditioning.* Biochim Biophys Acta, 2013. **1827**(5): p. 578-87.
15. Colavitti, R., et al., *Reactive oxygen species as downstream mediators of angiogenic signaling by vascular endothelial growth factor receptor-2/KDR.* J Biol Chem, 2002. **277**(5): p. 3101-8.
16. Don, A.S. and P.J. Hogg, *Mitochondria as cancer drug targets.* Trends Mol Med, 2004. **10**(8): p. 372-8.
17. Johnson, F. and C. Giulivi, *Superoxide dismutases and their impact upon human health.* Mol Aspects Med, 2005. **26**(4-5): p. 340-52.
18. Zorov, D.B., M. Juhaszova, and S.J. Sollott, *Mitochondrial ROS-induced ROS release: an update and review.* Biochim Biophys Acta, 2006. **1757**(5-6): p. 509-17.

19. Er, E., et al., *Mitochondria as the target of the pro-apoptotic protein Bax.* Biochim Biophys Acta, 2006. **1757**(9-10): p. 1301-11.
20. Tait, S.W. and D.R. Green, *Mitochondria and cell death: outer membrane permeabilization and beyond.* Nat Rev Mol Cell Biol, 2010. **11**(9): p. 621-32.
21. Begriche, K., et al., *Drug-induced toxicity on mitochondria and lipid metabolism: mechanistic diversity and deleterious consequences for the liver.* J Hepatol, 2011. **54**(4): p. 773-94.
22. Nadanaciva, S., et al., *Target identification of drug induced mitochondrial toxicity using immunocapture based OXPHOS activity assays.* Toxicol In Vitro, 2007. **21**(5): p. 902-11.
23. Pereira, C.V., et al., *Mitochondrial bioenergetics and drug-induced toxicity in a panel of mouse embryonic fibroblasts with mitochondrial DNA single nucleotide polymorphisms.* Toxicol Appl Pharmacol, 2012. **264**(2): p. 167-81.
24. Volkova, M. and R. Russell, 3rd, *Anthracycline cardiotoxicity: prevalence, pathogenesis and treatment.* Curr Cardiol Rev, 2011. **7**(4): p. 214-20.
25. Simunek, T., et al., *Anthracycline-induced cardiotoxicity: overview of studies examining the roles of oxidative stress and free cellular iron.* Pharmacol Rep, 2009. **61**(1): p. 154-71.
26. Sardao, V.A., et al., *Morphological alterations induced by doxorubicin on H9c2 myoblasts: nuclear, mitochondrial, and cytoskeletal targets.* Cell Biol Toxicol, 2009. **25**(3): p. 227-43.
27. Branco, A.F., et al., *Differentiation-dependent doxorubicin toxicity on H9c2 cardiomyoblasts.* Cardiovasc Toxicol, 2012. **12**(4): p. 326-40.
28. Octavia, Y., et al., *Doxorubicin-induced cardiomyopathy: from molecular mechanisms to therapeutic strategies.* J Mol Cell Cardiol, 2012. **52**(6): p. 1213-25.
29. Zhang, C., et al., *Resveratrol attenuates doxorubicin-induced cardiomyocyte apoptosis in mice through SIRT1-mediated deacetylation of p53.* Cardiovasc Res, 2011. **90**(3): p. 538-45.
30. Zhang, Y.W., et al., *Cardiomyocyte death in doxorubicin-induced cardiotoxicity.* Arch Immunol Ther Exp (Warsz), 2009. **57**(6): p. 435-45.
31. Huang, C., et al., *Juvenile exposure to anthracyclines impairs cardiac progenitor cell function and vascularization resulting in greater susceptibility to stress-induced myocardial injury in adult mice.* Circulation, 2010. **121**(5): p. 675-83.
32. De Angelis A, P.E., Cappetta D, Marino L, Filippelli A, Berrino L, Ferreira-Martins J, Zheng H, Hosoda T, Rota M, Urbanek K, Kajstura J, Leri A, Rossi F, Anversa P, *Anthracycline cardiomyopathy is mediated by depletion of the cardiac stem cell pool and is rescued by restoration of progenitor cell function.* Circulation, 2010. **121**: p. 276-292.
33. Von Hoff, D.D., et al., *Risk factors for doxorubicin-induced congestive heart failure.* Ann Intern Med, 1979. **91**(5): p. 710-7.
34. Sardao, V.A., et al., *Doxorubicin-induced mitochondrial dysfunction is secondary to nuclear p53 activation in H9c2 cardiomyoblasts.* Cancer Chemother Pharmacol, 2009. **64**(4): p. 811-27.
35. Menna, P., E. Salvatorelli, and G. Minotti, *Doxorubicin degradation in cardiomyocytes.* J Pharmacol Exp Ther, 2007. **322**(1): p. 408-19.

36. Vejpongsa, P. and E.T. Yeh, *Topoisomerase 2beta: a promising molecular target for primary prevention of anthracycline-induced cardiotoxicity.* Clin Pharmacol Ther, 2014. **95**(1): p. 45-52.
37. Carvalho, F.S., et al., *Doxorubicin-Induced Cardiotoxicity: From Bioenergetic Failure and Cell Death to Cardiomyopathy.* Med Res Rev, 2013.
38. Carvalho, R.A., et al., *Metabolic remodeling associated with subchronic doxorubicin cardiomyopathy.* Toxicology, 2010. **270**(2-3): p. 92-8.
39. Pereira, G.C., et al., *Mitochondrionopathy phenotype in doxorubicin-treated Wistar rats depends on treatment protocol and is cardiac-specific.* PLoS One, 2012. **7**(6): p. e38867.
40. Cole, M.P., et al., *The protective roles of nitric oxide and superoxide dismutase in adriamycin-induced cardiotoxicity.* Cardiovasc Res, 2006. **69**(1): p. 186-97.
41. Costantini, P., et al., *Modulation of the mitochondrial permeability transition pore by pyridine nucleotides and dithiol oxidation at two separate sites.* J Biol Chem, 1996. **271**(12): p. 6746-51.
42. Saeki, K., et al., *Doxorubicin directly binds to the cardiac-type ryanodine receptor.* Life Sci, 2002. **70**(20): p. 2377-89.
43. Kalivendi, S.V., et al., *Doxorubicin activates nuclear factor of activated T-lymphocytes and Fas ligand transcription: role of mitochondrial reactive oxygen species and calcium.* Biochem J, 2005. **389**(Pt 2): p. 527-39.
44. Lim, C.C., et al., *Anthracyclines induce calpain-dependent titin proteolysis and necrosis in cardiomyocytes.* J Biol Chem, 2004. **279**(9): p. 8290-9.
45. Duchen, M.R., A. Leyssens, and M. Crompton, *Transient mitochondrial depolarizations reflect focal sarcoplasmic reticular calcium release in single rat cardiomyocytes.* J Cell Biol, 1998. **142**(4): p. 975-88.
46. Zhao, Y., et al., *Redox proteomic identification of HNE-bound mitochondrial proteins in cardiac tissues reveals a systemic effect on energy metabolism after doxorubicin treatment.* Free Radic Biol Med, 2014. **72C**: p. 55-65.
47. Lagoa, R., et al., *The decrease of NAD(P)H:quinone oxidoreductase 1 activity and increase of ROS production by NADPH oxidases are early biomarkers in doxorubicin cardiotoxicity.* Biomarkers, 2014. **19**(2): p. 142-53.
48. Gilliam, L.A., et al., *The anticancer agent doxorubicin disrupts mitochondrial energy metabolism and redox balance in skeletal muscle.* Free Radic Biol Med, 2013. **65**: p. 988-96.
49. Oliveira, P.J., et al., *Carvedilol-mediated antioxidant protection against doxorubicin-induced cardiac mitochondrial toxicity.* Toxicol Appl Pharmacol, 2004. **200**(2): p. 159-68.
50. Santos, D.L., et al., *Carvedilol protects against doxorubicin-induced mitochondrial cardiomyopathy.* Toxicol Appl Pharmacol, 2002. **185**(3): p. 218-27.
51. Oliveira, P.J., M.S. Santos, and K.B. Wallace, *Doxorubicin-induced thiol-dependent alteration of cardiac mitochondrial permeability transition and respiration.* Biochemistry (Mosc), 2006. **71**(2): p. 194-9.
52. Mordente, A., et al., *New developments in anthracycline-induced cardiotoxicity.* Curr Med Chem, 2009. **16**(13): p. 1656-72.

53. Chandran, K., et al., *Doxorubicin inactivates myocardial cytochrome c oxidase in rats: cardioprotection by Mito-Q.* Biophys J, 2009. **96**(4): p. 1388-98.
54. Zhou, S., et al., *Cumulative and irreversible cardiac mitochondrial dysfunction induced by doxorubicin.* Cancer Res, 2001. **61**(2): p. 771-7.
55. Kim, Y., et al., *Anthracycline-induced suppression of GATA-4 transcription factor: implication in the regulation of cardiac myocyte apoptosis.* Mol Pharmacol, 2003. **63**(2): p. 368-77.
56. Suliman, H.B., et al., *The CO/HO system reverses inhibition of mitochondrial biogenesis and prevents murine doxorubicin cardiomyopathy.* J Clin Invest, 2007. **117**(12): p. 3730-41.
57. Kawamura, T., et al., *Expression of p300 protects cardiac myocytes from apoptosis in vivo.* Biochem Biophys Res Commun, 2004. **315**(3): p. 733-8.
58. Niu, J., et al., *Cardiac-targeted expression of soluble fas attenuates doxorubicin-induced cardiotoxicity in mice.* J Pharmacol Exp Ther, 2009. **328**(3): p. 740-8.
59. Kim, D.S., et al., *Plantainoside D protects adriamycin-induced apoptosis in H9c2 cardiac muscle cells via the inhibition of ROS generation and NF-kappaB activation.* Life Sci, 2007. **80**(4): p. 314-23.
60. Vedam, K., et al., *Role of heat shock factor-1 activation in the doxorubicin-induced heart failure in mice.* Am J Physiol Heart Circ Physiol, 2010. **298**(6): p. H1832-41.
61. Shan, Y.X., et al., *Hsp10 and Hsp60 modulate Bcl-2 family and mitochondria apoptosis signaling induced by doxorubicin in cardiac muscle cells.* J Mol Cell Cardiol, 2003. **35**(9): p. 1135-43.
62. Liu, J., et al., *ERKs/p53 signal transduction pathway is involved in doxorubicin-induced apoptosis in H9c2 cells and cardiomyocytes.* Am J Physiol Heart Circ Physiol, 2008. **295**(5): p. H1956-65.
63. Shizukuda, Y., et al., *Targeted disruption of p53 attenuates doxorubicin-induced cardiac toxicity in mice.* Mol Cell Biochem, 2005. **273**(1-2): p. 25-32.
64. Kurz, E.U., P. Douglas, and S.P. Lees-Miller, *Doxorubicin activates ATM-dependent phosphorylation of multiple downstream targets in part through the generation of reactive oxygen species.* J Biol Chem, 2004. **279**(51): p. 53272-81.
65. Tsang, W.P., et al., *Reactive oxygen species mediate doxorubicin induced p53-independent apoptosis.* Life Sci, 2003. **73**(16): p. 2047-58.
66. Nithipongvanitch, R., et al., *Mitochondrial and nuclear p53 localization in cardiomyocytes: redox modulation by doxorubicin (Adriamycin)?* Antioxid Redox Signal, 2007. **9**(7): p. 1001-8.
67. Yoshida, M., et al., *Chronic doxorubicin cardiotoxicity is mediated by oxidative DNA damage-ATM-p53-apoptosis pathway and attenuated by pitavastatin through the inhibition of Rac1 activity.* J Mol Cell Cardiol, 2009. **47**(5): p. 698-705.
68. Zhu, W., et al., *Acute doxorubicin cardiotoxicity is associated with p53-induced inhibition of the mammalian target of rapamycin pathway.* Circulation, 2009. **119**(1): p. 99-106.
69. Liu, X., et al., *Pifithrin-alpha protects against doxorubicin-induced apoptosis and acute cardiotoxicity in mice.* Am J Physiol Heart Circ Physiol, 2004. **286**(3): p. H933-9.
70. Feridooni, T., et al., *Cardiomyocyte specific ablation of p53 is not sufficient to block doxorubicin induced cardiac fibrosis and associated cytoskeletal changes.* PLoS One, 2011. **6**(7): p. e22801.

71. Simpson, C., H. Herr, and K.A. Courville, *Concurrent therapies that protect against doxorubicin-induced cardiomyopathy.* Clin J Oncol Nurs, 2004. **8**(5): p. 497-501.
72. Berthiaume, J.M. and K.B. Wallace, *Adriamycin-induced oxidative mitochondrial cardiotoxicity.* Cell Biol Toxicol, 2007. **23**(1): p. 15-25.
73. Al-Majed, A.A., et al., *Alpha-lipoic acid ameliorates myocardial toxicity induced by doxorubicin.* Pharmacol Res, 2002. **46**(6): p. 499-503.
74. Bast, A., et al., *Protection by flavonoids against anthracycline cardiotoxicity: from chemistry to clinical trials.* Cardiovasc Toxicol, 2007. **7**(2): p. 154-9.
75. Bast, A., et al., *Protectors against doxorubicin-induced cardiotoxicity: flavonoids.* Cell Biol Toxicol, 2007. **23**(1): p. 39-47.
76. Sack, M.N. and T. Finkel, *Mitochondrial metabolism, sirtuins, and aging.* Cold Spring Harb Perspect Biol, 2012. **4**(12).
77. Schumacker, P.T., *A tumor suppressor SIRTainty.* Cancer Cell, 2010. **17**(1): p. 5-6.
78. Verdin, E., et al., *Sirtuin regulation of mitochondria: energy production, apoptosis, and signaling.* Trends Biochem Sci, 2010. **35**(12): p. 669-75.
79. Frye, R.A., *Phylogenetic classification of prokaryotic and eukaryotic Sir2-like proteins.* Biochem Biophys Res Commun, 2000. **273**(2): p. 793-8.
80. Sauve, A.A., *Sirtuin chemical mechanisms.* Biochim Biophys Acta, 2010. **1804**(8): p. 1591-603.
81. Pereira, C.V., et al., *Regulation and protection of mitochondrial physiology by sirtuins.* Mitochondrion, 2012. **12**(1): p. 66-76.
82. Pirinen, E., G. Lo Sasso, and J. Auwerx, *Mitochondrial sirtuins and metabolic homeostasis.* Best Pract Res Clin Endocrinol Metab, 2012. **26**(6): p. 759-70.
83. Canto, C., et al., *Interdependence of AMPK and SIRT1 for metabolic adaptation to fasting and exercise in skeletal muscle.* Cell Metab, 2010. **11**(3): p. 213-9.
84. Sauve, A.A., et al., *The biochemistry of sirtuins.* Annu Rev Biochem, 2006. **75**: p. 435-65.
85. Chen, Y., et al., *Sirtuin-3 (SIRT3), a therapeutic target with oncogenic and tumor-suppressive function in cancer.* Cell Death Dis, 2014. **5**: p. e1047.
86. Kim, S.C., et al., *Substrate and functional diversity of lysine acetylation revealed by a proteomics survey.* Mol Cell, 2006. **23**(4): p. 607-18.
87. Hallows, W.C., B.N. Albaugh, and J.M. Denu, *Where in the cell is SIRT3?--functional localization of an NAD+-dependent protein deacetylase.* Biochem J, 2008. **411**(2): p. e11-3.
88. Scher, M.B., A. Vaquero, and D. Reinberg, *SirT3 is a nuclear NAD+-dependent histone deacetylase that translocates to the mitochondria upon cellular stress.* Genes Dev, 2007. **21**(8): p. 920-8.
89. Sundaresan, N.R., et al., *SIRT3 is a stress-responsive deacetylase in cardiomyocytes that protects cells from stress-mediated cell death by deacetylation of Ku70.* Mol Cell Biol, 2008. **28**(20): p. 6384-401.
90. Lombard, D.B., et al., *Mammalian Sir2 homolog SIRT3 regulates global mitochondrial lysine acetylation.* Mol Cell Biol, 2007. **27**(24): p. 8807-14.
91. Hirschey, M.D., et al., *SIRT3 regulates mitochondrial fatty-acid oxidation by reversible enzyme deacetylation.* Nature, 2010. **464**(7285): p. 121-5.

92. Palacios, O.M., et al., *Diet and exercise signals regulate SIRT3 and activate AMPK and PGC-1alpha in skeletal muscle.* Aging (Albany NY), 2009. **1**(9): p. 771-83.
93. Newman, J.C., W. He, and E. Verdin, *Mitochondrial protein acylation and intermediary metabolism: regulation by sirtuins and implications for metabolic disease.* J Biol Chem, 2012. **287**(51): p. 42436-43.
94. Hallows, W.C., et al., *Sirt3 promotes the urea cycle and fatty acid oxidation during dietary restriction.* Mol Cell, 2011. **41**(2): p. 139-49.
95. Schlicker, C., et al., *Substrates and regulation mechanisms for the human mitochondrial sirtuins Sirt3 and Sirt5.* J Mol Biol, 2008. **382**(3): p. 790-801.
96. Shulga, N., R. Wilson-Smith, and J.G. Pastorino, *Sirtuin-3 deacetylation of cyclophilin D induces dissociation of hexokinase II from the mitochondria.* J Cell Sci, 2010. **123**(Pt 6): p. 894-902.
97. Cimen, H., et al., *Regulation of succinate dehydrogenase activity by SIRT3 in mammalian mitochondria.* Biochemistry, 2010. **49**(2): p. 304-11.
98. Ahn, B.H., et al., *A role for the mitochondrial deacetylase Sirt3 in regulating energy homeostasis.* Proc Natl Acad Sci U S A, 2008. **105**(38): p. 14447-52.
99. Law, I.K., et al., *Identification and characterization of proteins interacting with SIRT1 and SIRT3: implications in the anti-aging and metabolic effects of sirtuins.* Proteomics, 2009. **9**(9): p. 2444-56.
100. Finkel, T., C.X. Deng, and R. Mostoslavsky, *Recent progress in the biology and physiology of sirtuins.* Nature, 2009. **460**(7255): p. 587-91.
101. Tanno, M., et al., *Emerging beneficial roles of sirtuins in heart failure.* Basic Res Cardiol, 2012. **107**(4): p. 273.
102. Shinmura, K., et al., *Caloric restriction primes mitochondria for ischemic stress by deacetylating specific mitochondrial proteins of the electron transport chain.* Circ Res, 2011. **109**(4): p. 396-406.
103. Lu, Z., et al., *SIRT3-dependent deacetylation exacerbates acetaminophen hepatotoxicity.* EMBO Rep, 2011. **12**(8): p. 840-6.
104. Pillai, V.B., et al., *Mitochondrial SIRT3 and heart disease.* Cardiovasc Res, 2010. **88**(2): p. 250-6.
105. Sundaresan NR, S.S., Pillai VB, Rajamohan SB, Gupta MP, *SIRT3 is a stress-responsive deacetylase in cardiomyocytes that protects cells from stress-mediated cell death by deacetylation of Ku70.* Mol Cell Biol., 2008.
106. Pillai, V.B., et al., *Exogenous NAD blocks cardiac hypertrophic response via activation of the SIRT3-LKB1-AMP-activated kinase pathway.* J Biol Chem, 2010. **285**(5): p. 3133-44.
107. Kim, H.S., et al., *SIRT3 is a mitochondria-localized tumor suppressor required for maintenance of mitochondrial integrity and metabolism during stress.* Cancer Cell, 2010. **17**(1): p. 41-52.
108. Kimes, B.W. and B.L. Brandt, *Characterization of two putative smooth muscle cell lines from rat thoracic aorta.* Exp Cell Res, 1976. **98**(2): p. 349-66.
109. Kimes, B.W. and B.L. Brandt, *Properties of a clonal muscle cell line from rat heart.* Exp Cell Res, 1976. **98**(2): p. 367-81.
110. Pereira, S.L., et al., *Metabolic remodeling during H9c2 myoblast differentiation: relevance for in vitro toxicity studies.* Cardiovasc Toxicol, 2011. **11**(2): p. 180-90.

111. Romero-Calvo, I., et al., *Reversible Ponceau staining as a loading control alternative to actin in Western blots.* Anal Biochem, 2010. **401**(2): p. 318-20.
112. Bao, J., et al., *Characterization of the murine SIRT3 mitochondrial localization sequence and comparison of mitochondrial enrichment and deacetylase activity of long and short SIRT3 isoforms.* J Cell Biochem, 2010. **110**(1): p. 238-47.
113. Samant, S.A., et al., *SIRT3 deacetylates and activates OPA1 to regulate mitochondrial dynamics during stress.* Mol Cell Biol, 2014. **34**(5): p. 807-19.
114. Dirks-Naylor, A.J., et al., *The effects of acute doxorubicin treatment on proteome lysine acetylation status and apical caspases in skeletal muscle of fasted animals.* J Cachexia Sarcopenia Muscle, 2013. **4**(3): p. 239-43.
115. Su, S., et al., *Sesamin ameliorates doxorubicin-induced cardiotoxicity: involvement of Sirt1 and Mn-SOD pathway.* Toxicol Lett, 2014. **224**(2): p. 257-63.
116. Ahmed, L.A. and S.A. El-Maraghy, *Nicorandil ameliorates mitochondrial dysfunction in doxorubicin-induced heart failure in rats: possible mechanism of cardioprotection.* Biochem Pharmacol, 2013. **86**(9): p. 1301-10.
117. Calenic, B., et al., *p53-Pathway activity and apoptosis in hydrogen sulfide-exposed stem cells separated from human gingival epithelium.* J Periodontal Res, 2013. **48**(3): p. 322-30.
118. Li, S., et al., *p53-induced growth arrest is regulated by the mitochondrial SirT3 deacetylase.* PLoS One, 2010. **5**(5): p. e10486.
119. Chae, H.J., et al., *Radiation protects adriamycin-induced apoptosis.* Immunopharmacol Immunotoxicol, 2005. **27**(2): p. 211-32.
120. Lai, H.C., et al., *Propofol ameliorates doxorubicin-induced oxidative stress and cellular apoptosis in rat cardiomyocytes.* Toxicol Appl Pharmacol, 2011. **257**(3): p. 437-48.
121. Tokudome, T., et al., *Ventricular nonmyocytes inhibit doxorubicin-induced myocyte apoptosis: involvement of endogenous endothelin-1 as a paracrine factor.* Endocrinology, 2004. **145**(5): p. 2458-66.
122. Cheng, Y., et al., *Interaction of Sirt3 with OGG1 contributes to repair of mitochondrial DNA and protects from apoptotic cell death under oxidative stress.* Cell Death Dis, 2013. **4**: p. e731.
123. Granados-Principal, S., et al., *Hydroxytyrosol ameliorates oxidative stress and mitochondrial dysfunction in doxorubicin-induced cardiotoxicity in rats with breast cancer.* Biochem Pharmacol, 2014. **90**(1): p. 25-33.
124. Pointon, A.V., et al., *Doxorubicin in vivo rapidly alters expression and translation of myocardial electron transport chain genes, leads to ATP loss and caspase 3 activation.* PLoS One, 2010. **5**(9): p. e12733.
125. Marfe, G., et al., *Kaempferol induces apoptosis in two different cell lines via Akt inactivation, Bax and SIRT3 activation, and mitochondrial dysfunction.* J Cell Biochem, 2009. **106**(4): p. 643-50.